BMC Biology

RESEARCH

Open Access

Uncovering protein prenylation in Th1 cells: novel prenylation sites and insights into statin and farnesyltransferase inhibition

Jana Koch[1,2,3], Alessandra Ruggia[1,4], Carina Beha[1], Irina Wipf[1], Damir Zhakparov[1,2], Patrick Westermann[1], Svenja Schmelzer[1], Anja Heider[1], Klemens Fröhlich[5] and Katja Baerenfaller[1,2*]

Abstract

Background T helper 1 (Th1) cell activation is an essential process for immune responses and is tightly regulated, including the prenylation of proteins critical for T cell function. Prenylation facilitates membrane association and protein function and, according to current consensus, is confined to C-terminal prenylation motifs. However, the full extent of the prenylated proteome, a broader understanding of prenylation sites, and the effects of inhibiting prenylation or blocking isoprenoid synthesis using statins remain incompletely understood. To address these gaps, we aimed to comprehensively identify and characterise protein prenylation in Th1 cells.

Results Using a click chemistry-based enrichment approach followed by mass spectrometry in primary in vitro-differentiated Th1 cells, we identified both known and novel prenylated proteins, some of which exhibited differential prenylation during Th1 cell activation, highlighting the dynamic nature of the Th1 prenylome. Characterisation of these proteins revealed isoform-specific prenylation, novel C-terminal prenylation motifs, and a structural motif associated with internal prenylation. Furthermore, statin treatment influenced the Th1 prenylome, altering protein prenylation in a prenyltransferase-dependent manner, underscoring distinct enzymatic specificities and potential off-target effects.

Conclusions Our findings confirm that prenylation plays a key role in Th1 cell function, with more proteins undergoing prenylation than previously known, some of which exhibit activation-dependent changes. The identification of non-canonical prenylation events challenges current views on prenylation, expanding the repertoire of modification sites. Together, our molecular insights into protein prenylation in Th1 cells and the effects of prenyltransferase inhibition and statin treatment have important implications for therapeutic strategies targeting immune regulation.

Keywords T cells, T helper 1 cells, Immunology, Autoimmunity, Statin, Prenylation, Geranylgeranylation, Farnesylation, Mass spectrometry, Click chemistry

*Correspondence:
Katja Baerenfaller
katja.baerenfaller@siaf.uzh.ch
Full list of author information is available at the end of the article

Background

T helper (Th) cells are key players in the adaptive immune system. Different subsets of Th cells, such as Th1 and Th2 cells, coordinate effective immune responses against specific groups of pathogens while also contributing to various immune disorders. For example, Th1 cells mediate responses against intracellular bacteria and viruses but can also promote autoimmune diseases when dysregulated in a pathological setting. Th cell activation is a highly regulated process that integrates multiple signals, leading to rapid cell differentiation, proliferation, migration, cytokine secretion, and metabolic adaptations. Among these adaptations, Th cell activation induces upregulation of the mevalonate pathway and differential prenylation of proteins essential for Th cell function [1–10]. Prenylation is a post-translational modification (PTM) in which either a 15-carbon farnesyl group or a 20-carbon geranylgeranyl group is conjugated to a cysteine residue of a target protein by a protein prenyltransferase (PTase). These enzymes include farnesyltransferase (FTase), geranylgeranyltransferase type I (GGTase-I), Rab geranylgeranyltransferase (RabGGTase or GGTase-II), and the more recently identified GGTase-III, each with distinct substrate and prenylation motif preferences [11–14]. The attachment of these large, hydrophobic lipids influences protein membrane localisation, protein–protein interactions, and the anchoring of proteins to specific subcellular compartments, thereby altering protein function [15, 16]. According to current consensus, the prenylated cysteine is located at the protein C-terminus, with the main prenylation motifs being CaaX or CXXX, where "a" represents an aliphatic residue (alanine, glycine, valine, leucine, or isoleucine), and "X" represents any amino acid. Additional annotated prenylation sites in the UniProt database are CXC, CCX, CC or C [17].

Protein prenylation plays a central role in numerous cellular processes, and its dysregulation is implicated in various diseases. For example, Hutchinson–Gilford progeria syndrome (HGPS) is caused by a mutant form of Lamin A, referred to as progerin, which permanently retains the farnesylated C-terminus that remains associated with the nuclear membrane and leads to structural changes. Similarly, the accumulation of constitutively farnesylated progerin-like proteins, resulting from impaired processing of Prelamin A by ZMPSTE24, causes a progeroid phenotype [18–20]. Oncogenic RAS family members, including KRAS, RHEB, and HRAS, rely on farnesylation for activation and membrane localisation, as this modification increases their lipophilicity and facilitates translocation to the plasma membrane, which is important in oncogenic signalling [21].

As a result, the use of geranylgeranyltransferase inhibitors (GGTIs) and farnesyltransferase inhibitors (FTIs) has emerged as a promising and effective therapeutic strategy. Following the demonstration of substantial therapeutic effects of the FTI Lonafarnib in HGPS and processing-deficient progeroid laminopathies, the drug was approved by the FDA in 2020 as the first farnesyltransferase inhibitor. Additional FTIs, as well as dual FTI and GGTase-I inhibitors, are currently in advanced stages of clinical development for the treatment of human cancers driven by oncogenic RAS family members and RAS-related proteins [22–26]. In this study, FTI-277 treatment was used to validate FTase targets and identify novel farnesylated proteins, as it has been shown to be highly selective for FTase over GGTase-I [27]. In addition to these specific inhibitors, statins indirectly inhibit prenylation by blocking the production of mevalonate, a precursor not only for cholesterol biosynthesis but also for the synthesis of prenyl groups. Statins, widely used for the prevention and management of cardiovascular diseases, have been included in the WHO Model Essential Medicines List since 2006 [28]. In 2018, an estimated 3.1% of the population across 83 countries used a lipid-modifying drug daily, with statins being the most frequently prescribed [29]. Their global utilisation continues to rise, with a 25% increase recorded between 2015 and 2020 [30]. While generally well tolerated, statins have been reported to cause off-target effects, including statin-induced myopathy in patients [31, 32]. In vitro experiments and studies in mice have shown that statin treatment inhibits the proliferation of activated T cells, peripheral blood mononuclear cells (PBMCs), and other cell types, as well as reduces TCR signalling [33–36]. Due to these effects, statins have been investigated for their immunomodulatory properties and potential treatment options in autoimmune and autoinflammatory diseases. However, findings from human studies have been inconclusive, leading to conflicting data regarding their benefits in multiple sclerosis [37]. To clarify these effects, it is essential to elucidate the molecular mechanisms underlying statin action, including their impact on protein prenylation.

Despite the critical role of protein prenylation, the extent of the prenylated proteome remains incompletely characterised. Currently, 174 human proteins are annotated as prenylated in the UniProt database, all of which are modified at their C-terminal consensus motifs in the canonical isoform, representing approximately 0.9% of the human proteome [17]. However, with the development of advanced enrichment and identification methods, recent studies have reported additional prenylated proteins and alternative modes of prenylation [12, 38–40], suggesting that the prenylome is broader than

previously recognised. These findings indicate the need for further research to systematically map the prenylated proteome and uncover non-canonical prenylation events. Enrichment methods for prenylated proteins often rely on metabolic labelling with azide- or alkyne-tagged isoprenoid analogues, followed by alkyne–azide cycloaddition, also referred to as click chemistry. This reaction covalently attaches the newly prenylated proteins to a moiety such as biotin or a resin, allowing subsequent enrichment, immobilisation, or fluorescent labelling. The prenylated proteins can then be identified, often using mass spectrometry-based proteomics [38, 41–45]. In this study, we aimed to comprehensively characterise the prenylome of in vitro-differentiated Th1 cells using a click chemistry-based enrichment strategy to capture newly prenylated proteins. By analysing the sites of prenylation, we challenged the current view of protein prenylation, identifying novel prenylation motifs and providing evidence for prenylation occurring outside the canonical C-terminal modification sites.

To better understand the molecular basis of statin effects on autoimmune diseases and how statins influence prenylation-dependent mechanisms in Th cells, we included statin treatment of Th1 cells to analyse its impact on the total protein profile and, specifically, on protein prenylation. Together, our findings provide new insights into protein prenylation and its regulatory role in Th1 cell biology, highlighting its potential relevance for immune function and therapeutic interventions.

Results

Identification of significantly enriched prenylated proteins in activated and non-activated Th1 cells

The experimental approach illustrated in Fig. 1A (left) was used to identify differentially enriched proteins in activated and non-activated in vitro-differentiated Th1 cells. This involved the addition of either geranylgeranyl alcohol azide (GG-Az) or farnesyl alcohol azide (F-Az) to the cells, followed by the use of click chemistry to covalently link the azide-labelled isoprenoid residues attached to newly prenylated proteins to a resin. The labelled proteins were then enriched and identified using mass spectrometry-based proteomics. As observed in the principal component analysis (PCA) of the enrichment samples, PC1 and PC2, which together account for 64.2% of the variance, show a clear separation between cells treated with GG-Az or F-Az and the mock-treated background control samples, while PC3 indicates a separation between activated and non-activated Th1 cells (Fig. 1B, C). In contrast, in the PCA of the total extract samples, there was a separation in PC1 between activated and non-activated Th1 cells, but no separation based on GG-Az, F-Az, or control treatment (Additional file 1: Fig. S1AB). This demonstrates that the enrichment of prenylated proteins using the click chemistry-based experimental approach was successful. Furthermore, this indicates that significant differences exist both in the total extracts and in the prenylated proteins between activated and non-activated Th1 cells.

In the statistical analyses comparing F-Az or GG-Az treated activated and non-activated Th1 cells to their respective background controls, a total of 287 significantly enriched prenylated proteins were identified (Additional file 1: Fig. S2). Of these, 145 proteins were exclusively identified in F-Az treated cells, 47 proteins exclusively in GG-Az treated cells, and 95 proteins both in F-Az and GG-Az treated cells (Additional file 1: Fig. S3, Additional file 2: Table S1). In line with our expectations, the overrepresented Gene Ontology Biological Process (GO-BP) categories among the significantly enriched prenylated proteins, compared to the background of all identified proteins, included processes related to protein membrane localisation and trafficking, primarily in Th1 cells treated with GG-Az. Additionally, the GO-BP category "Ras protein signal transduction" was predominantly overrepresented in Th1 cells treated with GG-Az, whereas in Th1 cells treated with F-Az, GO-BP terms associated with lipid metabolism were more prominently overrepresented. Immune-related GO-BP processes, including "leukocyte migration", were overrepresented in activated but not in non-activated Th1 cells (Additional file 1: Fig. S4).

Identification of significantly enriched prenylated proteins in activated Th1 cells treated or not with statin

In the experiment investigating the effect of statin treatment on Th1 cells, cells were pretreated with 0.75 μM Pitavastatin for 48 h or left untreated, alongside activation with anti-CD3/anti-CD28 antibodies. This was followed by incubation with GG-Az, F-Az, or mock treatment for an additional 24 h (Fig. 1A, right). The statin concentration and treatment conditions were optimised in prior titration experiments to achieve inhibition of proliferation with minimal cell death (Additional file 1: Fig. S5). The PCA of the top 500 variable proteins in the enrichment samples again showed a clear separation in PC1 and PC2 based on the isoprenoid treatment, accounting for 83.3% of the variance, while statin pretreatment resulted in the separation of samples in PC4 (Fig. 1D, E). In contrast, in the PCA of the total extract samples, statin pretreatment led to separation in PC2, accounting for 14.6% of the variance, while no separation was observed based on the isoprenoid treatment (Additional file 1: Fig. S1CD). This indicates that pretreatment with 0.75 μM Pitavastatin had a substantial impact on the protein profile of activated Th1 cells, corresponding

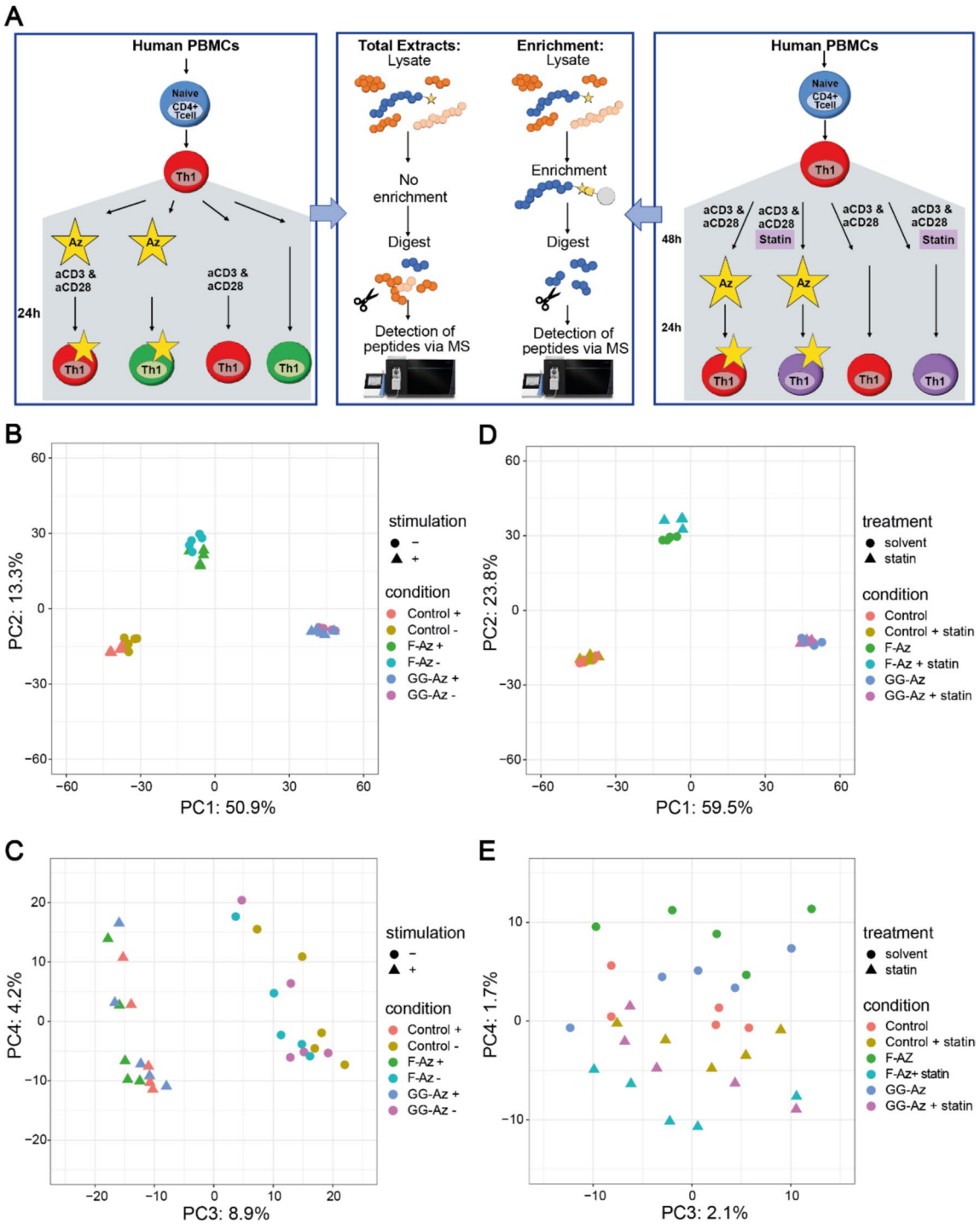

Fig. 1 **A** Experimental workflow for the identification of prenylated proteins in activated and non-activated Th1 cells treated with F-Az, GG-Az, or mock treatment (left), and in activated Th1 cells pretreated with statin or not, followed by treatment with F-Az, GG-Az, or mock treatment (right) ($N = 5$ biological replicates). **B** PC1 against PC2, and **C** PC3 against PC4 from the PCA of the top 500 variable proteins in the enrichment samples of activated and non-activated Th1 cells treated with GG-Az, F-Az or mock treatment. **C** PC1 against PC2, and **D** PC3 against PC4 from the PCA of the top 500 variable proteins in the enrichment samples of activated Th1 cells pretreated or not with statin and treated with GG-Az, F-Az, or mock treatment

to the observed significant reduction in cell proliferation (Additional file 1: Fig. S6), and had a considerable effect on protein prenylation.

Statistical analyses of proteins in the enrichment samples identified 270 proteins that were significantly enriched in Th1 cells pretreated with statin and treated with GG-Az compared to mock-treated cells. Similarly, 238 proteins were enriched in cells treated with GG-Az but without statin pretreatment, compared to mock-treated cells (Additional file 1: Fig. S7). Most of the significantly enriched proteins were shared between both conditions, with 49 proteins identified exclusively in statin-pretreated samples and only 17 proteins identified exclusively in non-statin-pretreated samples. In the F-Az-treated samples, compared to their respective background controls, 351 proteins were significantly enriched in statin-pretreated samples,

while 296 proteins were significantly enriched in non-statin-pretreated samples. Notably, 269 proteins were significantly enriched under both conditions (Additional file 1: Fig. S3, Additional file 2: Table S1).

The identified prenylated proteins contain both already known and novel prenylated proteins

For the bioinformatic analysis of the identified prenylated proteins, we considered all significantly enriched proteins in F-Az or GG-Az-treated Th1 cells, compared to their respective mock-treated controls, across both experiments depicted in Fig. 1A, that contained a cysteine in any isoform. Among the 636 putative prenylated proteins, 274 were exclusive to F-Az treatment, 159 to GG-Az treatment, and 203 were common to both treatments (Additional file 1: Fig. S8).

To compile a list of all known prenylated proteins, we performed a SPARQL query on UniProt to identify all farnesylated and geranylgeranylated proteins [17]. Additionally, we included the farnesylated proteins ULK3, DCAF8, CEP85, LRRF1, NAP1L4, RHBT3, and DPCD, as reported by Storck et al. [39], and GNAI1 and GNAI2, as reported by Palsuledesai et al. [38] in the list of known prenylated proteins. Of all the known prenylated proteins, 78 (42.6%) were identified in our experiments (Additional file 1: Fig. S9). From the perspective of the 636 identified prenylated proteins, 78 (12.3%) are already annotated as prenylated in UniProt (Additional file 1: Fig. S10), which is significantly more (p-value = 2.49e-76) than one would expect from randomly identifying this number of known prenylated proteins. This indicates that the experimental set-up indeed led to a significant enrichment of prenylated proteins.

Of the identified novel prenylated proteins, 234 were identified as only farnesylated, 144 as only geranylgeranylated, and 180 as both geranylgeranylated and farnesylated (Additional file 1: Fig. S11). Interestingly, comparing the known and the novel identified proteins gave 34 proteins that are known to be prenylated, but with a different moiety as in our experiments (Additional file 3: Table S2). Of the proteins with a discrepancy, 21 were found in our experiments in both F-Az- and GG-Az-treated samples, and 9 were found in F-Az-treated samples, despite being annotated as geranylgeranylated. This discrepancy might be explained by the fact that exogenously provided farnesol can be converted inside the cells into farnesyl diphosphate (FPP)-Az, which can subsequently be conjugated by geranylgeranyl pyrophosphate synthase with isopentenyl-PP to form GGPP-Az, a substrate for GGTases [46]. The identification of CNP and GNAI2, which are annotated as farnesylated, in GG-Az-treated cells cannot be easily explained by metabolic conversion of the substrates. Instead, it is likely due to the ability of GGTase-I to transfer both geranylgeranyl and farnesyl moieties, with the choice of the prenyl group depending on the protein acceptor [21, 47]. Notably, we also detected YKT6 in both GG-Az- and F-Az-treated cells, despite its annotation as farnesylated in UniProt (Fig. 2). However, a recent study has shown that YKT6 can undergo double prenylation, as its mono-farnesylated form is a substrate for GGTase-III [12]. Moreover, RHOB, which was identified only in F-Az-treated cells but is annotated as both farnesylated and geranylgeranylated, has been reported to alter its function and cellular localisation depending on whether it is geranylgeranylated or farnesylated [48]. These findings further support the validity of our measurements in detecting interesting prenylation patterns.

Prenylation at canonical prenylation motifs

Assessing the C-terminal amino acid sequences of the 636 identified prenylated proteins, only 30 had the canonical CaaX motif, while 45 had a CXXX motif in their canonical isoform, and 9 in one of their alternative isoforms (Additional file 2: Table S1). Interestingly, the alternative NAP1L4b isoform (Q99733-2) contains a large C-terminal arm with a C-terminal CKQQ motif, which is missing in the canonical NAP1L4 sequence. The other ubiquitously expressed nucleosome assembly protein family member NAP1L1, which is known to be farnesylated [41], also encodes a C-terminal CKQQ motif. Since we have observed in these cells that the NAP1L4b isoform is expressed, and NAP1L4 was previously reported to be farnesylated [39], it is likely that farnesylated Nap1L4b is present in Th1 cells.

When querying the sequences of all 174 proteins annotated as prenylated in UniProt [17], we found not only the expected CaaX (53 proteins) and CXXX (89 proteins) motifs but also the additional motifs CXC

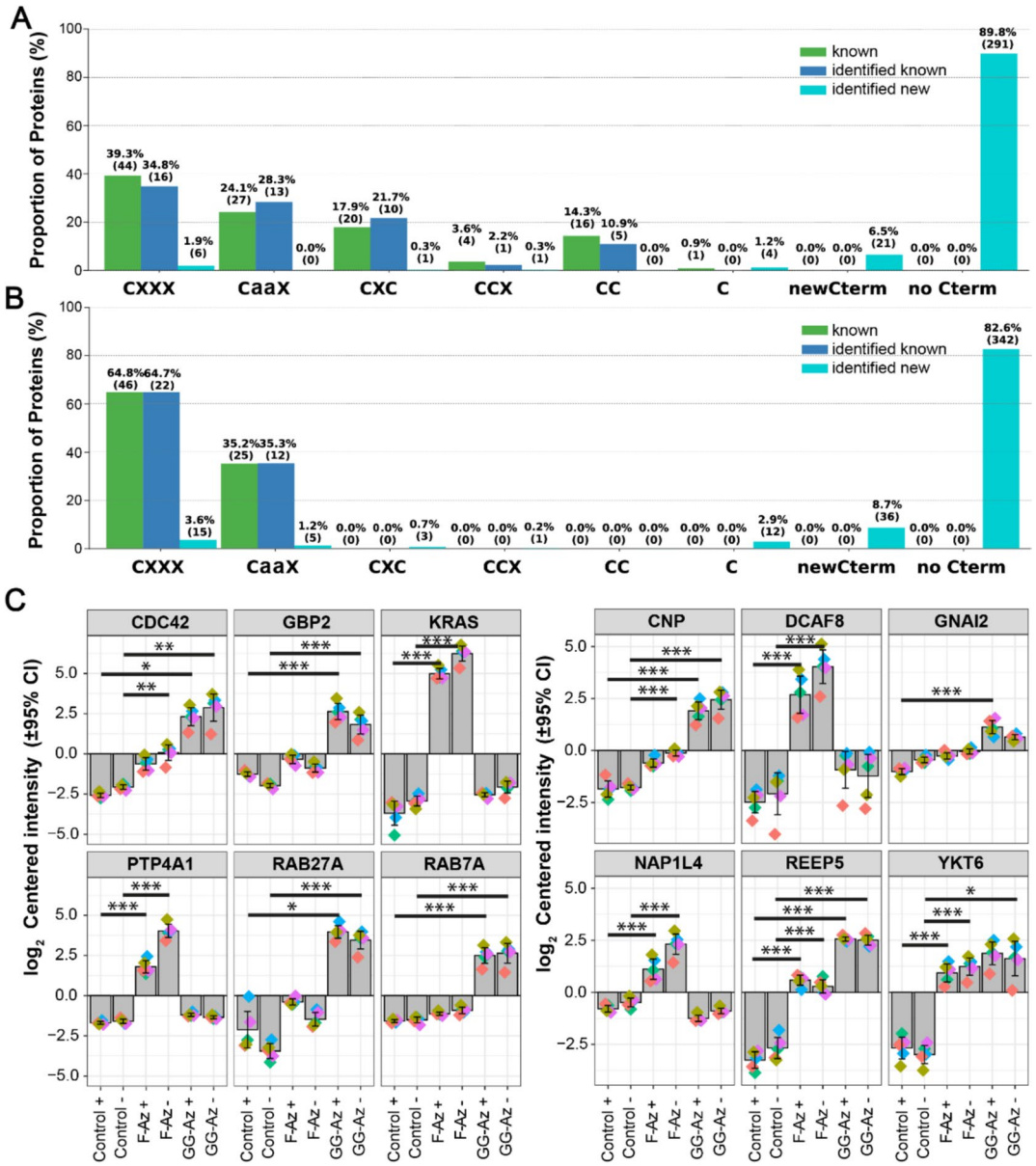

Fig. 2 Distribution of the canonical prenylation motifs, the new C-terminal prenylation motifs, and prenylation without a C-terminal cysteine in known prenylated proteins (green), identified prenylated proteins (blue), and newly identified prenylated proteins (cyan) in samples treated with **A** GG-Az and **B** F-Az. **C** Log_2-transformed centred intensities ± 95% confidence intervals for the identified prenylated proteins, as indicated, in activated (+) and non-activated (–) Th1 cells treated with GG-Az, F-Az, or mock-treated as controls. Stars indicate significant enrichment when comparing GG-Az- or F-Az-treated samples with their respective background controls (*** = *p*-value < 0.001, ** = *p*-value < 0.01, * = *p*-value < 0.05). The different colours of the diamonds represent different donors

(20 proteins), CC (16 proteins), CCX (4 proteins), and C (1 protein; RAB41), where "X" represents any amino acid except cysteine. These additional motifs are also considered canonical in this context. These are mainly thought to be substrates for GGTase-II, which can add two geranylgeranyl groups to two neighbouring cysteine residues [14]. Of the 636 identified prenylated proteins, 117 have a canonical prenylation motif in their sequence, and 14 of these do not have this motif in their main isoform.

In the previously known geranylgeranylated proteins, the most common canonical prenylation motif is CXXX, followed by CaaX, CXC, and CC. A similar pattern is observed in the known prenylated proteins identified in GG-Az-treated samples. In contrast, only 6 (1.9%) of the newly identified proteins in the GG-Az-treated

samples contain a CaaX or CXXX motif, and 3 (0.93%) a CXC, CCX, or C motif (Fig. 2A). The previously known farnesylated proteins all contain either a CXXX or a CaaX motif. These two motifs were also found in 20 (4.8%) of the newly identified farnesylated proteins. In addition, 16 (3.9%) contained the canonical prenylation motifs CXC [3], CCX [1], or C [12] (Fig. 2B).

One of the newly identified geranylgeranylated proteins detected in several enrichment samples is REEP5. The canonical isoform of this protein lacks a C-terminal prenylation motif, but its second isoform (Q00765-2) contains a CXX prenylation motif. Other examples of geranylgeranylated proteins identified in this study include the known geranylgeranylated proteins CDC42 and GBP2, as well as the RAB proteins RAB7A and RAB27A, both of which contain a CXC prenylation motif. The identified farnesylated proteins include the well-known KRAS, along with DCAF8 and the previously mentioned NAP1L4, both of which were recently reported as farnesylated [39] (Fig. 2C). In summary, of the 558 newly identified prenylated proteins, 40 (7.17%) contained a canonical prenylation motif: 28 (11.7%) in the newly identified 234 proteins in F-Az-treated samples, 3 (2.08%) in the newly identified 144 proteins in GG-Az-treated samples, and 9 (5%) both in samples treated with GG-Az or F-Az. Of the proteins in the human proteome that are not known to be prenylated, 1363 (5.3%) proteins contain a canonical prenylation motif. The presence of a canonical prenylation motif in the newly identified proteins is therefore overrepresented (p-value = 0.011), indicating true additional prenylation.

The sequence logos [49] of the last ten C-terminal amino acids of known farnesylated and geranylgeranylated proteins with a CaaX or CXXX motif show a preference for a polar or aliphatic amino acid at the last C-terminal amino acid. N-terminal to the cysteine, polar and positively charged amino acids dominate, except in farnesylated proteins with a CXXX motif, where no clear pattern is observed. The presence of polar and positively charged amino acids upstream of the prenylated cysteine corresponds to previously reported findings that both a conserved C-terminal polybasic region and prenylation motif are required for proper subcellular localisation and biological activity of PRL phosphatases [50]. Moreover, in the positions preceding or following the cysteine in the CXXX motif, or only preceding the cysteine in the CaaX motif, additional cysteines appear, suggesting the presence of the additional motifs CCXXX and CCXX, which might lead to double prenylation. For the CXXX motif, the amino acid following the cysteine is usually polar or positively charged, and for the additional canonical motifs CXC, CCX, and CC, polar amino acids and glycine dominate around and between the cysteines (Additional file 1: Fig. S12). Similar patterns were observed in the subset of known prenylated proteins identified here (Additional file 1: Fig. S13). Among these is PTP4A1, also called PRL-1, which contains a CaaX motif and is known to be farnesylated (Fig. 2C). The newly identified farnesylated proteins with the CaaX motif and the geranylgeranylated proteins with the CXXX motif also showed an upstream polybasic region, while the newly identified farnesylated proteins with a CXXX motif again showed no clear pattern upstream of the cysteine (Additional file 1: Fig. S14). This consistency in the amino acid distribution patterns around the canonical C-terminal prenylation motifs suggests that the newly identified prenylated proteins containing canonical prenylation motifs are also likely to be prenylated.

There is more prenylation beyond canonical prenylation motifs

For the 519 remaining proteins that do not contain any of the canonical prenylation motifs in any of their isoforms, a total of 935 distinct isoforms exists. Next, we determined the most protein C-terminal positions of cysteines in all their 935 distinct isoforms or only considering one isoform per protein. In the histogram using one isoform per protein, a high number of proteins had their most C-terminal cysteine in positions $-2, -3$, and -5 (Additional file 1: Fig. S15). This corresponded with the appearance of additional cysteines around the cysteine in the CaaX and CXXX motifs observed for the known and the newly identified prenylated proteins. We therefore defined the C-terminal CCC, CX, CXX, and CXXXX motifs with cysteines in positions $-1, -2, -3$, or -5 as new prenylation motifs. These new C-terminal prenylation motifs were contained in 44 proteins (Additional file 3: Table S3).

The remaining 474 proteins, which lack a cysteine in the last 5 C-terminal amino acids in any of their isoforms, were classified as internally prenylated proteins. Of these, 184 were significantly enriched only in samples treated with F-Az, 133 only in samples treated with GG-Az, and 157 in samples treated with F-Az or GG-Az. Moving forward, only the canonical isoform of these proteins was considered, except for four proteins in which the canonical isoform lacked a cysteine. In these cases, the isoform with the highest number of cysteines was selected. For the internally prenylated proteins, we next assessed the overrepresentation of the CC, CXC, and CCC motifs. Among proteins significantly enriched in samples treated with GG-Az, the CCC motif was predominantly overrepresented compared to the background, whereas for proteins enriched in samples treated with F-Az, the CC motif was mainly overrepresented.

Of the internally prenylated proteins, 22 had exactly one possibly prenylated cysteine, indicating the site of prenylation, with 20 in their canonical isoform (Additional file 3: Table S4). These proteins are mainly localised in organelle membranes and membrane protein complexes. To determine the likely site of prenylation in other proteins with multiple internal cysteines, we used the prediction-aware part-sphere exposure (pPSE) metric established by Bludau and colleagues. This metric describes the accessibility of amino acids by considering the number of neighbouring amino acids within a given distance in Ångströms while accounting for the predicted aligned error (PAE) value of the AlphaFold2 structure [51–53]. Relying on proteins with AlphaFold2 structures restricts the analysis to the canonical isoforms of the proteins. We found that the optimal distance was 30 Å, as at this distance, all cysteines in the single-cysteine prenylated proteins had a pPSE value of 0, meaning that they had no neighbouring amino acids within this distance. For the 462 internally prenylated proteins with a predicted AlphaFold2 structure, we calculated the accessibility of the cysteines, determined the lowest pPSE value, and counted how many cysteines had this lowest value. With this, we identified 204 internally prenylated proteins with exactly one most accessible cysteine. Of these, 20 are the aforementioned proteins with exactly one possibly prenylated cysteine in their canonical isoform, 5 had one single cysteine that was not in an annotated disulfide bridge, 130 had one cysteine with no neighbours (pPSE = 0), and 49 had one cysteine with the lowest pPSE (Additional file 2: Table S1).

Analysing structural motifs

Assessing the distribution of amino acids around the potentially prenylated cysteines in internally prenylated proteins revealed no specific patterns compared to the background distribution of comparable cysteines in proteins identified in the total extract samples but not in the enrichment samples (Additional file 1: Fig. S16). This observation remained consistent when we analysed peptides identified only in samples treated with GG-Az or F-Az, or both, in samples treated with GG-Az or F-Az (Additional file 1: Fig. S17). We therefore next assessed the structural context of residues at different positions around the cysteine residues using Foldseek. In Foldseek, a 3Di alphabet, here represented by Greek letters, describes the tertiary contacts between a residue and the residue of its nearest neighbour in three-dimensional space. It thus translates the three-dimensional amino acid conformation of proteins into a two-dimensional sequence of tertiary structures [54]. These sequences of tertiary structures were used to calculate the frequencies of the different 3Di states at each of the five positions surrounding the cysteines, for both prenylated cysteines and those in the background sequences (Fig. 3A, B). Analysing the percentage distribution of the different 3Di states for the putative prenylated cysteines and their surrounding residues, and testing for over-representation compared to the background, revealed a significant over-representation of the β state and an under-representation of the δ state at the putative prenylated cysteine. The δ state was also significantly under-represented at position + 5. Additional over-represented 3Di states included the ρ state at position − 1, as well as the ι and ς states at position + 1 (Fig. 3C). A Fisher's exact test on the distribution of all 3Di states at each position, using Monte Carlo simulation, confirmed a significantly different distribution at the position of the cysteine and at positions − 1 and + 1. From this, we conclude that prenylation requires not only the cysteine to be accessible but also the presence of a specific structural motif surrounding the putative prenylation site.

Treatment with farnesyl transferase inhibitor confirms prenylation of novel farnesylated proteins

To verify the prenylation status of farnesylated proteins, in vitro-differentiated Th1 cells were pre-treated or not with 20 μM farnesyl transferase inhibitor FTI-277 for 1 h. This concentration was determined in a previous titration experiment, as it showed a significant effect on proliferation without a significant impact on cell viability (Additional file 1: Fig. S18). Following this, cells were incubated with F-Az or subjected to mock treatment for an additional 23 h. As in previous experiments, both total protein extracts and samples enriched for prenylated proteins were subsequently analysed using mass spectrometry. The PCA of the enrichment samples shows separation along PC1, which contributes to 45.2% of the variance, distinguishing samples treated with F-Az from mock-treated samples. Along PC2, which explains 11.6% of the variance, the enrichment samples are further separated based on pre-treatment with FTI-277 (Additional file 1: Fig. S19).

Of the 49 proteins that were significantly less farnesylated upon FTI treatment, 31 are known to be prenylated, and 40 were identified as significantly enriched in samples treated with F-Az in the two previous experiments. The proteins that are not known to be prenylated but were found here to be less farnesylated upon FTI treatment and previously identified in F-Az-treated samples are RABGAP1, EHBP1L1, INF2, PRICKLE3, APOL3, CEP85L, FAM219A, MAPKAPK3, SPDL1, and WDTC1 (Fig. 4A, Additional file 3: Table S5). The proteins that are less farnesylated upon FTI treatment can be classified into five main categories. The first category comprises small GTPases, including RHEB, RAB28, RAP2A,

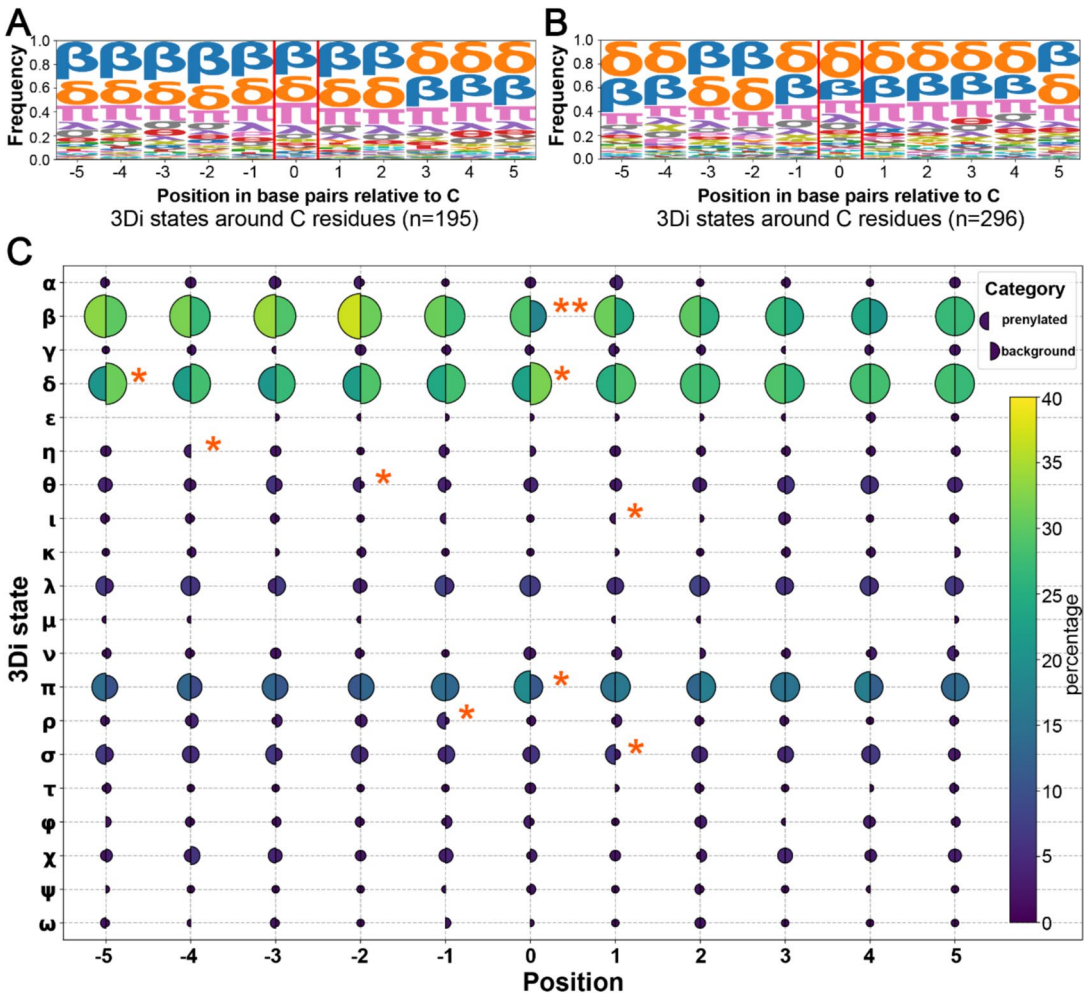

Fig. 3 **A** Sequence logos representing the 3Di states of the 184 putative internal prenylated cysteines along with the 5 amino acids upstream and downstream. **B** The same as in **A**, but for the 296 most accessible cysteines from the background proteins identified in total extracts but not in the enrichment samples. **C** For each position, the percentage distribution of each 3Di state was calculated and visualised using half-circles: the left half represents the percentage in the putative prenylated sequences (**A**), and the right half represents the percentage in the background sequences (**B**). Higher percentages are shown as larger half-circles in yellow and green, while lower percentages appear as smaller half-circles in blue, according to the indicated colour scale. Red asterisks indicate the statistical significance of the over-representation of specific 3Di states at specific positions, based on a hypergeometric test; the double asterisk "**" denotes a *p*-value < 0.01, and the single asterisk "*" denotes a *p*-value < 0.1

NRAS, RAP2C, KRAS, HRAS, and RRAS2, which are known prenylated proteins. The second category includes proteins associated with small GTPases, such as RIC1, RABGAP1, EHBP1L1, and IMA1, which are mostly not known to be prenylated. The third group consists of the lamins Lamin A, B1, and B2, a family of proteins that are well-established substrates for farnesylation. The fourth category encompasses members of the DNAJ homolog superfamily A (DNAJA), which act as co-chaperones and are also known to undergo prenylation. Finally, the fifth group includes a diverse set of proteins, such as the hormone receptor activator WBP2; the GTPases GNGT2 and GBP1; YKT6; the kinases MAPKAPK3 and ULK3; cytoskeletal organisation proteins like CEP85, CENPF, and INF2; and the ubiquitin-protein ligase complex substrate receptor DCAF8. Interestingly, the proteins RAP2C, RHOH, and ZFAND2B, which are annotated as geranylgeranylated but were significantly enriched only in F-Az-treated samples in both previous experiments, were also found to be significantly less abundant following FTI treatment (Additional file 3: Table S5).

Analysing the prenylation sites of farnesylated proteins sensitive to FTI treatment identifies a C-terminal single cysteine as the prenylation motif for the canonical isoform of RABGAP1. Examination of the sequences of the four RABGAP1 isoforms reveals that two isoforms

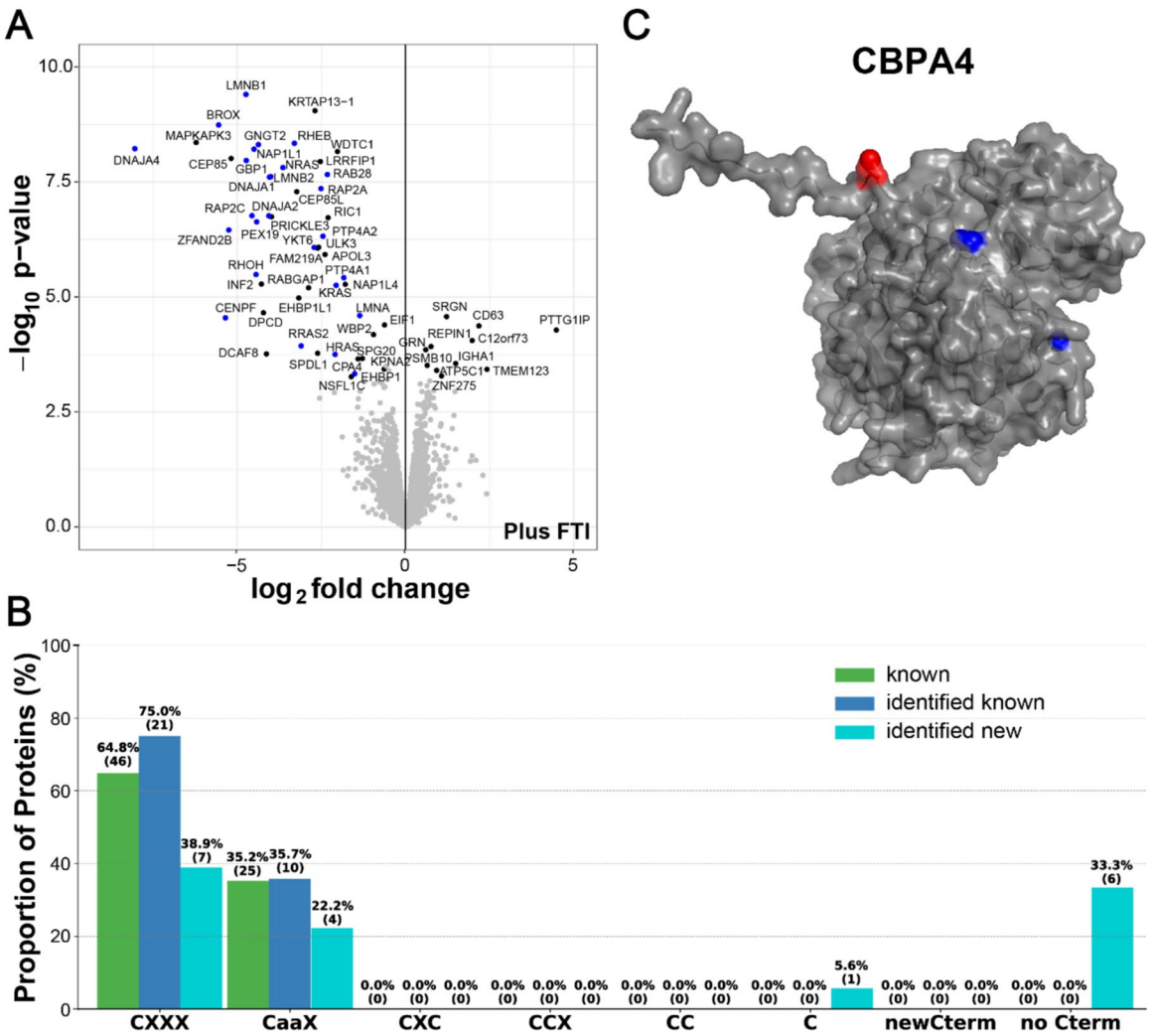

Fig. 4 **A** Volcano plot comparing prenylation-enriched proteins from in vitro-differentiated Th1 cells that were either pre-treated or not with the farnesyl transferase inhibitor (FTI-277) and subsequently treated with F-Az. Significantly different prenylated proteins are shown in blue; novel ones in black. **B** Distribution of prenylation motifs in known farnesylated proteins (green) and the 49 proteins significantly less farnesylated upon FTI treatment, categorised into identified known farnesylated proteins (blue) and newly identified farnesylated proteins (cyan). **C** 3D structure of CBPA4 as predicted by AlphaFold2, with the most accessible cysteine, located in a turn, shown in red, while less accessible cysteines are depicted in blue

possess a C-terminal CX motif, while the third isoform (Q9Y3P9-3) features the classical CXXX motif. In addition to Q9Y3P9-3, 28 of the identified FTI-sensitive farnesylated proteins contain the CXXX motif, including seven newly identified prenylated proteins, and fourteen proteins contain the CaaX motif, four of which are novel prenylated proteins (Fig. 4B) This distribution of motifs in farnesylated proteins sensitive to treatment with FTI-277, which specifically targets FTase [27], mirrors the preference of FTase for CaaX and CXXX sequences. Six of the identified FTI-sensitive farnesylated proteins contain an internal prenylation site. Using the above-mentioned methods, the most accessible cysteine could be determined for one of them, CBPA4, where it is located at position 16 (Fig. 4C).

Identification of proteins that are differentially prenylated between activated and non-activated Th1 cells

To uncover specific insights into the role of protein prenylation in Th1 cell biology, we next focused on differences in prenylated proteins in activated and non-activated Th1 cells. Initially, we analysed total protein extracts to gain an overview of differential protein expression between these conditions. We identified 251 proteins that were more abundant in activated Th1 cells, including JUNB, REL, EGR2, IRF4, BCL2L1, HMGCS1,

and the known prenylated proteins RAB27A and GBP2. Conversely, 258 proteins were more abundant in non-activated Th1 cells, including SELL and BID (Additional file 3: Table S6). These findings suggest an upregulation of anti-apoptotic proteins promoting cell survival and processes associated with prenylation during Th1 cell differentiation and activation.

To identify differentially prenylated proteins, we first compared enrichment samples of activated and non-activated Th1 cells treated with either F-Az or GG-Az, identifying 179 proteins with significant differences. We then excluded the 74 proteins that also showed significant differences between activated and non-activated control cells without isoprenoid addition, as these could reflect activation-dependent changes in protein levels. Following the same logic and to ensure the identification of truly prenylated proteins, we further excluded 86 proteins that overlapped with the 509 differentially expressed proteins in total extracts. After filtering, we obtained 63 differentially prenylated proteins, with 41 more prenylated in activated cells and 22 in non-activated cells (Additional file 3: Table S7, Additional file 2: Table S8). Of these, seven are known to be prenylated. Notably, none of the background-filtered proteins were known to be prenylated, supporting the validity of our approach in identifying differential prenylation independent of protein abundance changes. However, it remains possible that proteins with substantial abundance changes were not detected in the total extracts and that some proteins may undergo both abundance changes and differential prenylation.

In the F-Az-treated cells, 24 proteins were more prenylated in activated Th1 cells and 13 in non-activated cells. These include the known prenylated protein GNG12 among those more prenylated in activated cells and GBP1, RAB28, PTP4A1, and RHOH among those more prenylated in non-activated cells (Figs. 2C and 5A). Interestingly, GBP1, RAB28, PTP4A1, and RHOH were also found to be significantly less farnesylated upon FTI treatment, along with INF2, which contains a CaaX prenylation motif but has not been previously reported as prenylated (Additional file 2: Table S5). In the GG-Az-treated cells, 13 proteins showed increased prenylation in non-activated Th1 cells, including the known prenylated protein CRACR2A, while 24 proteins were more prenylated in activated Th1 cells, including the known prenylated protein GNG4 (Fig. 5B).

Subjecting the proteins showing increased prenylation in activated Th1 cells to a functional overrepresentation analysis using STRING [55] against the background of all proteins identified in the enrichment samples results in a cluster of G proteins including GNG12, GNG4, and GNAQ, and of cell surface receptors, such as TNFRSF25 regulating lymphocyte homeostasis, CD44, CD63, and CD82, which results in the overrepresentation of the GO Cellular Component (GO-CC) terms "Heterotrimeric G-protein complex" and "Side of membrane" (Additional file 1: Fig. S20). The STRING analysis of the proteins with increased prenylation in non-activated Th1 cells and 10 added interactors results in a highly interconnected cluster of proteins assigned to the GO-BP term "T cell activation" and the KEGG Pathway "T cell receptor signalling pathway" (Additional file 1: Fig. S21, S22). Notably, among the nine interactors added by STRING to this cluster, four are differentially expressed in total extracts: LAT is upregulated in activated Th1 cells, while SELL (CD62L), SH2D1A, and ITGAL (CD11a) are more highly expressed in non-activated cells. In non-activated Th1 cells, we therefore identified a closely interconnected network of proteins with increased prenylation, whose interaction partners exhibit changed abundance. This suggests a tightly regulated signalling network, influenced both by changes in protein localisation and interactions through prenylation, as well as by alterations in the abundance of interacting proteins.

The effect of statin treatment on protein prenylation is complex

Statin pretreatment of Th1 cells without the subsequent addition of isoprenoids led to a significant increase in the abundance of 19 proteins in total protein samples, with only SPOCK2, SLX4, and RAB11FIP1 not known to be prenylated. Among the three downregulated proteins GBP2, GFM2, and MED12, GBP2 is known to be prenylated (Additional file 1: Fig. S23A, Additional file 2: Table S9). This suggests that statin-induced abundance changes preferentially affect prenylated proteins in Th1 cell activation. When Th1 cells were first pre-treated with statin and subsequently F-Az or GG-Az was added, 63 and 59 proteins were upregulated, respectively, compared to Th1 cells without statin pretreatment (Additional file 1: Fig. S23BC, Additional file 2: Table S9). Notably, among the 77 additional statin-induced proteins in isoprenoid-treated cells, only 7 are known to be prenylated, while among the additional 22 downregulated proteins, only GBP1 is known to be prenylated. This indicates that additional mechanisms play a role when statin pretreatment is combined with isoprenoid addition. The functional analysis of the differentially expressed proteins in activated Th1 cells without added isoprenoids, performed using gene set enrichment analysis (GSEA) [56, 57], revealed that statin treatment affects pathways related to cell differentiation, exocytosis, and secretion (Additional file 1: Fig. S23D). When isoprenoids were added after statin pretreatment, the main overrepresented processes included oxidative phosphorylation, the

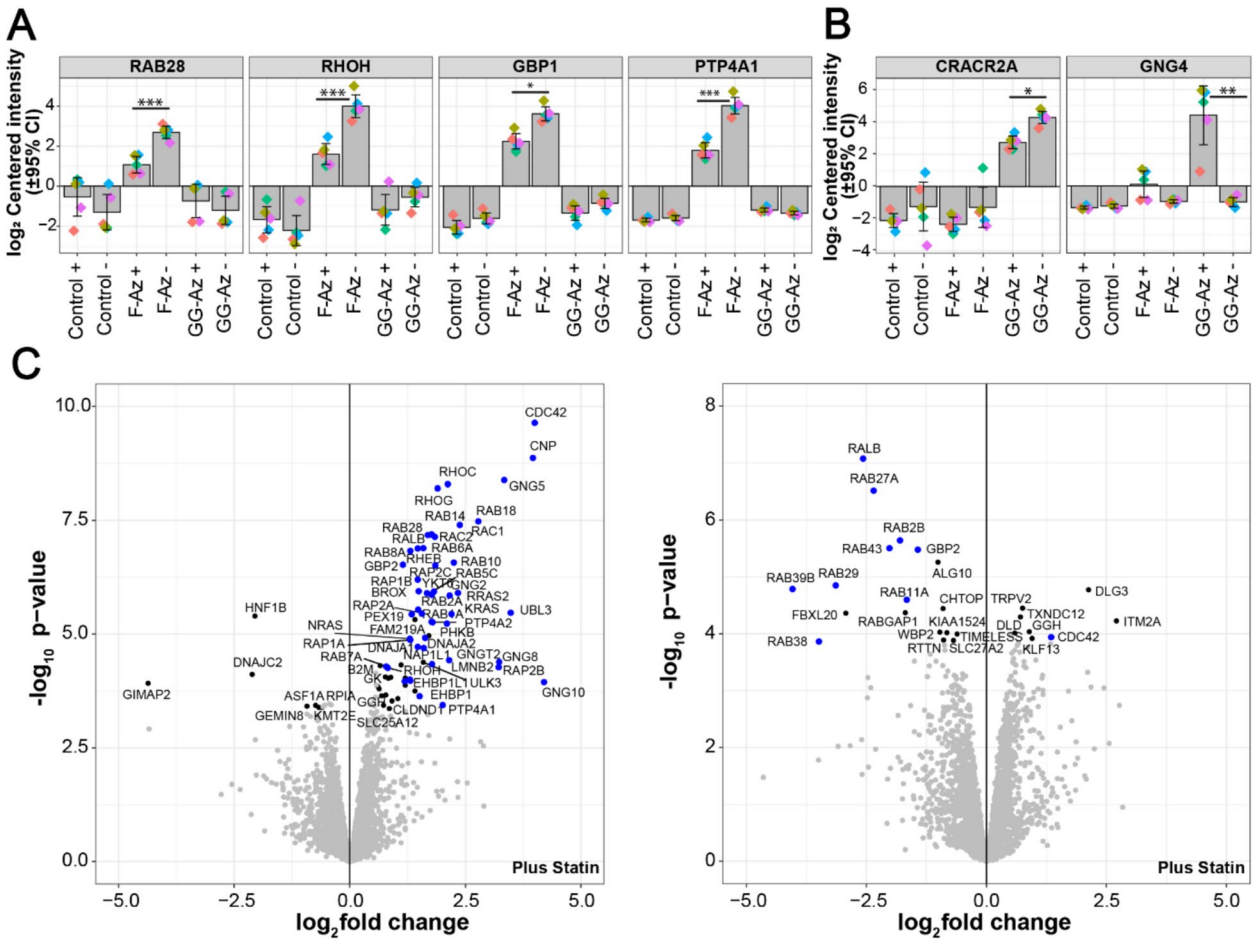

Fig. 5 For a selection of significantly prenylated proteins in enrichment samples of Th1 cells treated with **A** F-Az or **B** GG-Az, the $\log_2$-transformed centered intensities ± 95% confidence intervals are shown, as indicated, in activated (+) and non-activated (–) Th1 cells treated with GG-Az, F-Az, or mock-treated as controls. Stars indicate significant enrichment when comparing GG-Az- or F-Az-treated samples with their respective background controls (*** = p-value < 0.001, ** = p-value < 0.01, * = p-value < 0.05). The different colours of the diamonds represent different donors. **C** Volcano plots of prenylation enrichment samples comparing activated Th1 cells pre-treated or not with statin and subsequently treated with F-Az (left) and GG-Az (right). Bold dots indicate significantly changed proteins with or without pre-treatment with statin. Blue dots represent proteins already known to be prenylated

electron transport chain, and respiration, which are associated with cellular energy supply (Additional file 1: Fig. S23EF).

When analysing the enrichment samples comparing Th1 cells pretreated or not with statin, we observed strikingly different, and in some cases opposing, enrichment patterns in cells treated with F-Az or GG-Az (Fig. 5C). In F-Az-treated samples, 7 proteins were significantly less abundant after statin pretreatment, while 78 proteins were significantly more abundant. Among these, 11 proteins were also significantly more abundant in the total extracts of statin-pretreated control cells and were filtered out. Of the remaining 67 significantly enriched proteins in statin-pretreated, F-Az-treated samples, 51 (76%) are known to be prenylated, including KRAS, RHEB, DCAF8, NAP1L1, and NAP1L4. For KRAS, we observed a slower-migrating unprenylated proteoform in Western blots of PBMCs treated for 48 h with Pitavastatin, particularly upon restimulation of the cells, confirming the statin-induced prenylation deficit ((Additional file 1: Fig. S24). In contrast, none of the significantly enriched proteins in non-pretreated samples are known to be prenylated. In GG-Az-treated samples; however, the prenylation pattern was notably different. Only 11 proteins were significantly enriched in statin-pretreated samples, of which 8 remained after background filtering. Among these, only CDC42 is known to be prenylated. On the other hand, 22 proteins were more enriched in samples not pretreated with statin. Since the protein levels of the three proteins that changed significantly in total extracts

shifted in the opposite direction, they were retained. Of the 22 proteins significantly enriched in GG-Az-treated samples without statin pretreatment, 13 (59%) are known to be prenylated, including GBP2 and RALB, which were also significantly enriched in statin-pretreated, F-Az-treated samples (Additional file 2: Table S10).

These differences in the enrichment patterns are also evident in STRING network analyses [55]. In the proteins enriched in statin-pretreated, F-Az-treated Th1 cells compared against the background of all proteins identified in the enrichment samples, the Reactome Pathways "RAB geranylgeranylation" and "G beta:gamma signalling through CDC42" were most overrepresented, along with pathways associated with signal transduction and signalling, as well as the Gene Ontology Cellular Component (GO-CC) term "Plasma membrane" (Additional file 1: Fig. S25). In contrast, no significant enrichment was observed in the enriched proteins from statin-pretreated, GG-Az-treated Th1 cells. Instead, the Reactome Pathway "RAB geranylgeranylation" was significantly enriched in non-statin-pretreated, GG-Az-treated cells (Additional file 1: Fig. S26). This suggests that inhibiting isoprenoid biosynthesis, followed by supplementation with F-Az, leads to the expected increase in protein prenylation. In contrast, supplementation with GG-Az did not produce the same effect, possibly due to additional impacts of Pitavastatin on geranylgeranylation, such as the inhibition of RabGGTases.

Discussion

Protein prenylation plays a central role in numerous cellular processes. Disruption of this PTM typically results in a loss of protein function, owing to impaired protein interactions, mislocalisation, or a combination of both. Given its critical role, protein prenylation has become a promising therapeutic target, with several PTase inhibitors currently being tested for the treatment of various diseases [23]. Consequently, systematically mapping the prenylated proteome and its alterations under different conditions or upon inhibition is an important area of research, as it is essential for understanding the molecular mechanisms underlying these effects.

In this study, we employed a click chemistry-based enrichment approach combined with mass spectrometry to investigate protein prenylation in primary Th1 cells. This allowed us to identify both known and novel prenylated proteins. Additionally, we identified proteins that exhibited differential prenylation during Th1 cell activation. Proteins with increased prenylation were predominantly associated with G-protein complexes and membranes, while those with decreased prenylation were overrepresented in the pathway "Modulators of TCR Signalling and T Cell Activation". This highlights the pivotal role of protein prenylation in regulating Th1 cell activation, a key process in immune regulation.

A protein that was consistently identified as farnesylated in our experiments, sensitive to FTI treatment, and more prenylated in non-activated Th1 cells is RHOH. RHOH is predominantly expressed in haematopoietic cells and belongs to the Rho GTPase family. It is constitutively active and GTP-bound, inhibiting NFκB and CRK/p38 activation by TNF, as well as the activities of RAC1, RHOA, and CDC42. Additionally, RHOH functions as an adapter molecule in TCR signalling, facilitating the efficient interaction of ZAP70 with the LAT signalosome, thereby regulating T cell activation, development, and functional differentiation. Given its critical role, reduced RHOH levels or RHOH mutations have been implicated in the pathology of autoimmune diseases [58–62]. RHOH contains the C-terminal CKIF sequence, a CXXX prenylation motif, which is essential for its localisation interactions with ZAP70. Although it is annotated as geranylgeranylated in UniProt based on inference from sequence similarity [17], an in vitro assay has shown that RHOH is a target for FTase [63]. Interestingly, RHOB, which contains the C-terminal CKVL sequence, has been reported to undergo either farnesylation or geranylgeranylation, depending on the cellular context [48, 64]. However, in our study, RHOB was exclusively identified as farnesylated.

Another group of proteins known to undergo farnesylation are the lamins. In our experiments, Lamin B1 and B2 were identified in enrichment samples from both activated and non-activated Th1 cells treated with F-Az. They were also identified as farnesylated both in activated Th1 cells pretreated or not with statin, followed by F-Az treatment, with significantly increased farnesylation observed upon statin pre-treatment. Furthermore, Lamin B1 and B2 were found to be significantly less farnesylated after treatment with FTI-277, along with Lamin A, which was not identified as farnesylated in the other experiments. As increased farnesylation of Lamin A, either through the progerin mutation of the *LMNA* gene or impaired processing of prelamin A, causes various laminopathies, the FTI Lonafarnib was approved by the FDA in 2020 for the treatment of HGPS and processing-deficient progeroid laminopathies [22].

The farnesylation of oncogenic RAS family members, including KRAS, RHEB, and HRAS, is also of high clinical importance. In our experiments, KRAS, HRAS, and RHEB were identified as farnesylated in both activated and non-activated Th1 cells, as well as in activated Th1 cells pretreated with statin. Only HRAS did not reach statistical significance in activated Th1 cells without statin pretreatment, while KRAS and RHEB were found to be significantly more farnesylated following statin

pretreatment. Furthermore, the farnesylation of KRAS, HRAS, and RHEB was found to be sensitive to treatment with FTI-277. Given the direct link between farnesylation and the oncogenic potential of these proteins, its inhibition has been the focus of extensive clinical research, resulting in several promising therapeutic strategies. Notably, the FTI Tipifarnib, which disrupts the function of HRAS and RHEB, has been granted Breakthrough Therapy Designation by the FDA following a successful clinical trial [24, 25]. Since KRAS can become geranylgeranylated and remain functional in FTI-treated cells, dual FTI and GGTase-I inhibitors such as FGTI-2734 have the potential to target KRAS-driven human cancers [21, 65].

Given the context of protein lipidation, another PTM that becomes relevant is palmitoylation, as it also involves cysteine modifications, but occurs through thioester bond formation, which is characteristic of palmitoylation, rather than the more stable thioether bond formation observed in prenylation. Interestingly, the single-cysteine protein SEC61B, which is annotated as palmitoylated based on its detection in the acyl-RAC assay, a method that cleaves thioester bonds in palmitoylated cysteines and captures the freed thiols [66], was identified here as farnesylated. Another protein identified as internally farnesylated in our experiments is ALDH9A1. Notably, internal prenylation of ALDH9A1 has been previously reported, occurring through a thioester linkage of cysteine with farnesal or geranylgeranial, which are degradation products of prenylated proteins, thereby adding a reversible prenoyl modification [67]. Thus, SEC61B could potentially be prenylated through a thioester bond rather than being palmitoylated.

Determining the precise type of cysteine-linked lipid modification in the relevant cellular contexts will be a crucial area of future research, particularly in the context of inhibiting prenylation or palmitoylation for therapeutic applications.

In addition to identifying the precise type of lipid modification, it is also important to re-examine the sites of modification. In the UniProt database [17], 174 human proteins are currently annotated as prenylated. Notably, all annotated farnesylated proteins contain either a CXXX or CaaX prenylation motif, while the annotated geranylgeranylated proteins have 6 C-terminal prenylation motifs. The evidence codes provided in UniProt [17] for the annotation of prenylated proteins are predominantly based on manual assertion (using sequence similarity, sequence model evidence, or curator inference) or experimental evidence. Since proteins identified in enrichment experiments are typically filtered for the presence of a prenylation motif before being reported, this introduces a bias towards known prenylation motifs. As a result, these known motifs are reinforced while previously unrecognised motifs remain underrepresented. In our experiments, we identified novel farnesylated proteins with canonical C-terminal prenylation motifs that are typically associated with geranylgeranylated proteins. Additionally, we discovered new C-terminal prenylation motifs in proteins newly identified as farnesylated or geranylgeranylated. Furthermore, we identified proteins with internal prenylation, where the putative internal prenylation sites appear to show a structural prenylation motif rather than a sequence-based motif around the modified cysteine.

Expanding the repertoire of known prenylation motifs, both canonical and newly identified, is likely to increase the number of annotated farnesylated and geranylgeranylated proteins. In turn, this will help reduce annotation bias by informing future predictions, ultimately leading to more comprehensive identification and annotation of protein prenylation.

An important aspect of protein prenylation annotation is the presence of protein isoforms with different sequences that impact potential prenylation sites. The examples identified here include the farnesylated NAP1L4, where only the alternative NAP1L4b isoform contains a C-terminal CXXX prenylation motif; the geranylgeranylated REEP5, where the second isoform contains a CXX prenylation motif; and the farnesylated RABGAP1, where different isoforms contain a C-terminal C, CX, or CXXX motif. Similarly, CRACR2A, which showed reduced geranylgeranylation upon Th1 cell activation, exhibits isoform-specific prenylation: only the canonical CRACR2A-A isoform contains the C-terminal GTPase domain and a CCX prenylation motif, both of which are absent in the shorter CRACR2A-C isoform. CRACR2A prenylation has been shown to be crucial for TCR signalling and membrane localisation, while deprenylation leads to cytoplasmic localisation and protein degradation [8].

If only specific isoforms contain consensus prenylation motifs, differential splicing and isoform expression might serve as a specialised mechanism for altering protein function and localisation through differential prenylation. Quantifying the relative expression of different isoforms in different cellular contexts could therefore be of interest. Additionally, different isoform sequences should be considered when investigating protein prenylation.

For the statin treatment, our hypothesis was that proteins most affected in Th1 cell activation due to limitations in the prenylation pathway caused by statin pretreatment would achieve a high level of de novo prenylation after the exogenous addition of the substrates F-Az or GG-Az. This was indeed observed after the addition of F-Az, as many known prenylated proteins were enriched in statin-pretreated, F-Az-treated

samples, with various pathways associated with signal transduction and signalling being overrepresented. Interestingly, the proteins enriched in the F-Az-treated samples were also associated with the Reactome pathway "RAB geranylgeranylation" For example, GNG4, GNG5, and GNG8, which are usually geranylgeranylated, were identified in statin-pretreated and F-Az-treated cells. This may again be explained by the metabolic conversion of exogenously provided farnesol to form GGPP-Az, a substrate for GGTases [46]. Alternatively, some prenylated proteins might undergo alternative prenylation by FTase or GGTase-I under restrictive conditions [21, 68]. In contrast, in cells treated with GG-Az, known prenylated proteins were primarily enriched in the samples not pretreated with GG-Az. This striking difference might be explained by additional effects of Pitavastatin on geranylgeranylation, including the potential inhibition of RabGGTase, which would account for the increased prenylation of RAB proteins in non-statin-pretreated cells. This mode of action is supported by the observation that other lipophilic statins, but not the hydrophilic statin Pravastatin, directly inhibit UBIAD1, a membrane prenyltransferase that mediates the geranylgeranylation of various substrates and has been shown to regulate HMG-CoA reductase [69, 70]. Alternatively, GDI1, which interacts with RHOH and several RAB proteins, where it inhibits GDP dissociation and promotes the dissociation of GDP-bound RAB proteins from membranes [62], might be inhibited. Elucidating the molecular basis of treatment effects of various statins on protein geranylgeranylation in Th1 cells, along with additional off-target effects in various systems, could provide valuable insights into the underlying mechanisms of these off-target effects and help explain previously observed, partially conflicting findings.

Conclusions

Our investigation into protein prenylation has unveiled numerous novel findings, emphasising the power of this approach in expanding our understanding of this critical PTM. By applying click chemistry-based enrichment combined with mass spectrometry, we not only confirmed known prenylated proteins but also identified new ones, broadening our understanding of the prenylated proteome in Th1 cells. Importantly, analysing differential prenylation during Th1 cell activation revealed a network of prenylated proteins tightly linked to the LAT signalosome, emphasising the functional role of prenylation in T cell signaling and immune regulation.

A major finding of this study is that the conventional focus on consensus CaaX and CXXX prenylation motifs is too narrow, leading to the overlooking and underreporting of many prenylated proteins. Our data demonstrate that additional C-terminal motifs, especially for farnesylated proteins, must be considered. Additionally, we provide evidence supporting the existence of internal prenylation sites, which follow a structural rather than a sequence-based prenylation motif. These insights call for a re-evaluation of current annotation criteria for protein prenylation and suggest that annotation databases should expand beyond traditional motifs to improve the accuracy of prenylation predictions, including the annotation of prenylated non-canonical protein isoforms.

In addition, investigating the effect of statin treatment on protein prenylation uncovered that statin treatment enhanced the detection of prenylated proteins in F-Az-treated samples, but it also revealed a previously unrecognised off-target effect on protein geranylgeranylation. These findings highlight the need for a more nuanced understanding of how prenylation inhibitors affect protein function across different biological systems.

Taken together, our study opens new avenues for future research, providing a refined perspective on protein prenylation that extends beyond established paradigms. Given the increasing use of prenylation inhibitors as therapeutic agents, a more comprehensive understanding of the molecular effects and compensatory changes in prenylation will be crucial for optimising targeted therapies. Our findings emphasise the need for broader and more systematic approaches to studying prenylation in various biological and disease contexts, ultimately enhancing the precision and efficacy of interventions targeting this essential PTM.

Methods

Cell Isolation and culture

PBMCs were isolated from whole blood as previously described [71]. Naïve $CD4^+$ T cells were isolated using the Naïve $CD4^+$ T Cell Isolation Kit II, human (Miltenyi Biotec, Bergisch Gladbach, Germany), and the autoMACS Pro Separator (Miltenyi Biotec, Bergisch Gladbach, Germany). After isolation, cells were cultured at 1 million cells/ml in AIM-V medium (Thermo Fisher Scientific Inc., Waltham, USA) and stimulated with plate-bound anti-CD3 (1 µg/ml) and anti-CD28 (1 µg/ml) antibodies (in-house production) to induce activation. IL-2 (10 ng/ml) (StemCell Technologies Canada Inc., Vancouver, Canada), IL-12 (25 ng/ml) (StemCell Technologies Canada Inc., Vancouver, Canada), and anti-IL-4 antibody (5 µg/ml) (R&D Systems, Minneapolis, USA) were added to the culture to drive Th1 cell differentiation. Cells were incubated at 37 °C with 5% CO_2. After 3 days, the medium was replaced with complete RPMI containing 10% heat-inactivated fetal calf serum (Merck, Darmstadt, Germany), 1×penicillin/streptomycin (Sigma-Aldrich,

St. Louis, MO, USA), 1×vitamins (Sigma-Aldrich, St. Louis, MO, USA), 1×sodium pyruvate solution (Sigma-Aldrich, St. Louis, MO, USA), and 1% MEM non-essential amino acids (Sigma-Aldrich, St. Louis, MO, USA) in RPMI-1640 (Lonza, Basel, Switzerland), including IL-2 and IL-12 at the concentrations specified above. When indicated, cells were reactivated using plate-bound anti-CD3 and anti-CD28 antibodies in complete RPMI, supplemented with IL-2, IL-12, and anti-IL-4 antibody.

Labelling of prenylated proteins in Th1 cells

For the comparison of activated and non-activated Th1 cells, Th1 cells were stimulated as described above on day 6 to activate them, while non-activated cells were kept resting. At the same time, to label prenylated proteins, cells were treated with F-Az dissolved in ethanol (25 nM) (Cayman Chemical, Ann Arbor, USA) or GG-Az dissolved in DMSO (25 nM) (Thermo Fisher Scientific Inc., Waltham, USA), or the respective solvent as a control, for 24 h before harvesting. Cells were washed in PBS, and pellets were frozen in liquid nitrogen and stored at − 80 °C until further use.

FTI treatment of Th1 cells

To identify proteins that are sensitive to farnesyl transferase inhibition, Th1 cells were cultured, stimulated on day 6 as described above, and treated with FTI-277 (20 µM) (Selleck Chemicals LLC, Houston, USA) for 1 h before adding F-Az or ethanol (control) for 23 h, followed by harvesting. Of note, due to a power failure, the culturing conditions during the last few hours of the experiment were not controlled. Cell proliferation and viability were assessed using an H3-thymidine incorporation assay and PI staining.

Statin treatment of Th1 cells

To identify prenylation changes due to statin treatment in Th1 cell activation, Th1 cells were stimulated on days 6 and 13, and treated with Pitavastatin (0.75 µM) in DMSO or DMSO alone (control) added on day 13 for 48 h. Then, F-Az, GG-Az, or EtOH and DMSO as their respective solvent controls were added for 24 h before harvesting. The effect of Pitavastatin treatment on cell viability and proliferation was monitored using an H3-Thymidine incorporation assay and propidium iodide (PI) staining.

Preparation of total extracts

For the analysis of the total proteome of Th1 cells, 1 million cells per sample were lysed in urea extraction buffer and prepared for mass spectrometry measurements, essentially as previously described [72].

Enrichment of prenylated proteins

For the enrichment of prenylated proteins, the Click-iT™ Protein Enrichment Kit (Thermo Fisher Scientific Inc., Waltham, USA) was used. Per sample, 50 million cells were processed. In brief, azide-labelled proteins were covalently linked to resin-bound alkyne via a click reaction. The bound peptides were washed several times before on-resin digestion with trypsin. The resulting tryptic peptides were then purified and desalted using Pierce C18 Spin Columns (Thermo Fisher Scientific Inc., Waltham, USA).

Mass spectrometry measurements

Peptide concentrations of the total extracts were measured using the Pierce Quantitative Colorimetric Peptide Assay Kit, and approximately 250 ng per sample were measured on an Orbitrap Eclipse Mass Spectrometer (Thermo Scientific, USA) coupled to an Easy nLC 1200 (Thermo Scientific, USA). Samples were passed through an Acclaim(TM) PepMap(TM) 100 C18 in-line pre-column (5 µm particle size, 0.1 mm diameter, 150 mm length, Thermo Scientific, USA) before reverse-phase peptide separation on a NanoLC column with integrated emitter (75 µm inner diameter×25 cm length×365 µm outer diameter packed with Reprosil-Pur 120 C18 beads with 1.9 µm diameter, CoAnn Technologies, USA) located in a pre-column heater (PRSO-V2 from Sonation, Thermo Scientific, USA). Buffer A is 0.1% formic acid in water, and Buffer B is 0.1% formic acid in 80% acetonitrile. Peptides were eluted at a flow rate of 200 nl/min using a linear gradient of varying lengths. Survey Scan parameters were as follows: Scan Range: 350–2000 m/z, Orbitrap Resolution: 120,000, normalised AGC target: 100%, Microscans: 1. Filter options were used: Peptide, charge 2–7, excluding undetermined charge states. Dynamic exclusion was set to 60 s with a mass tolerance of ± 10 ppm. Minimum intensity was set to 1e4. MS2 scans were recorded with the following settings: Isolation Window, 1.6; Collision Energy, 27%; Detector Type, LIT; Scan Rate, rapid; Maximum Injection Time, 50 ms; normalised AGC Target, 100%. Enrichment samples were injected twice. The exact acquisition parameters are part of the raw files that are accessible at the MassIVE web server (Availability of data and materials).

Data analysis

After mass spectrometry measurements, the mass spectra were matched to peptides using MaxQuant version 2.0.3.1 [73], using the parameters: match between runs enabled, cysteine carbamidomethylation as fixed modification, oxidation of methionine, acetylation of the protein N-terminus, and cyclisation of N-terminal glutamine

to pyroglutamate as variable modifications, allowing for a maximum of 3 modifications per peptide [74]. Trypsin/P was added as digestion enzyme, and 2 missed cleavages were allowed. The database used for searching was the human reference database UP000005640 not including isoforms downloaded from UniProt [17] with contaminants included. Label-free quantification was performed. The peptide and protein FDRs were kept at 1%.

Further analyses were conducted using R including DEP [75] and other specified packages. Only proteins that were identified in more than 50% of samples in one condition were analysed further; missing data were imputed using the minimal deterministic imputation as implemented in the MSnbase package in R for enrichment samples [76]. For total extracts, proDA was used instead of imputation [77]. Differential expression analysis was performed using limma through the integration of the DEP package, with the following significance cutoffs: FDR < 0.05 and FC > 1.5. Graphs were generated using ggplot2.

Proteins were considered prenylated if they were significantly more abundant in enrichment samples treated with F-Az or GG-Az compared to their respective mock-treated controls and contained a cysteine in at least one of their isoforms.

Analysis of prenylated proteins

Known prenylated proteins were retrieved from the UniProt database using SPARQL queries, and protein sequences were obtained from UniProt in FASTA format for sequence-based analyses [17]. Motif assessment and analysis were conducted using custom Python scripts. Sequence logos were generated in PSSMSearch [78] using unweighted frequency-based representation. To assess the structural context of internal prenylation sites, StructureMap [53] was used to annotate cysteine residue accessibility, with structural exposure assessed by the pPSE value at a 30 Ångström distance setting without smoothing. Additionally, FoldSeek [54] was utilised to investigate the structural environments of prenylation sites at the tertiary structure level. FoldSeek translates tertiary protein structures into a 3Di structural alphabet, encoding spatial relationships between amino acid residues. Protein structures were retrieved in PDB format from the AlphaFold database [51].

The entire computational pipeline, including SPARQL queries, motif discovery scripts, and structural analyses, is documented in Jupyter Notebooks (Availability of data and materials).

Pymol

Pymol version 2.5.5 was used under an academic licence [79]. Protein structures were loaded from Alphafold2 using the UniProt identifier and the Alphafold2import plugin [52].

Abbreviations

F-Az	Farnesyl alcohol azide
FPP	Farnesyl diphosphate
FTase	Farnesyltransferase
FTI	Farnesyltransferase inhibitor
GG-Az	Geranylgeranyl alcohol azide
GGTase	Geranylgeranyltransferase
GGTI	Geranylgeranyltransferase inhibitor
GO-BP	Gene Ontology Biological Process
GO-CC	Gene Ontology Cellular Component
GSEA	Gene set enrichment analysis
HGPS	Hutchinson–Gilford progeria syndrome
PAE	Predicted aligned error
PBMC	Peripheral blood mononuclear cell
PCA	Principal component analysis
pPSE	Prediction-aware part-sphere exposure
PTase	Prenyltransferase
PTM	Post-translational modification
Th cell	T helper cell

Supplementary Information

The online version contains supplementary material available at https://doi.org/10.1186/s12915-025-02345-1.

Additional file 1: Figures S1–S26. Fig. S1-PCA plots of the top 500 most variable proteins in total extract samples from experiment 1 with activated and non-activated Th1 cells. Fig. S2-Volcano plots of enrichment samples from experiment 1 with activated and non-activated Th1 cells. Fig. S3-Venn diagrams showing the overlaps between the significantly enriched proteins in samples from experiments 1 and 2. Fig. S4-Enriched GO-BP terms in the significantly enriched prenylated proteins in samples from experiment 1 with activated and non-activated Th1 cells. Fig. S5-Assessment of Pitavastatin kinetics and determination of optimal concentrations. Fig. S6-Analysis of Th1 cell viability and cell proliferation upon Pitavastatin treatment. Fig. S7-Volcano plots of enrichment samples from experiment 2 with activated Th1 cells pretreated or not with statin. Fig. S8-Venn diagram illustrating significantly enriched farnesylated and geranylgeranylated proteins. Fig. S9-Proportion of identified known prenylated proteins relative to all annotated prenylated proteins. Fig. S10-Comparison of identified and annotated prenylated proteins. Fig. S11-Venn diagram with the number of newly identified prenylated proteins in cells treated with GG-Az, F-Az, or both. Fig. S12-Sequence logos of the 10 most C-terminal amino acids of the proteins known to be farnesylated or geranylgeranylated. Fig. S13-Sequence logos of the 10 most C-terminal amino acids of the proteins known to be prenylated and identified here as significantly enriched. Fig. S14-Sequence logos of the 10 most C-terminal amino acids of the proteins not previously known to be prenylated and identified here as significantly enriched. Fig. S15-Histograms of the most C-terminal cysteine positions. Fig. S16-Sequence logos of 15-residue windows centred on the cysteine for potentially internally prenylated and background proteins. Fig. S17-Sequence logos of 15-residue windows centred on the cysteine for potentially internally prenylated proteins, separated by farnesylation and geranylgeranylation. Fig. S18-Assessment of optimal concentrations of the farnesyl transferase inhibitor FTI-277. Fig. S19-PCA plots of prenylation enrichment samples from Th1 cells pre-treated or not with the farnesyl transferase inhibitor FTI-277. Fig. S20-Cluster 3 from the STRING analysis of the proteins showing increased prenylation in activated Th1 cells compared to non-activated Th1 cells. Fig. S21-Cluster 3 from the STRING analysis of the proteins showing increased prenylation in activated Th1 cells compared to non-activated Th1 cells. Fig. S22-STRING network analysis of the 22 proteins with increased prenylation in non-activated Th1 cells compared to activated Th1 cells plus 10 interactors. Fig. S23-Proteome changes in response to statin treatment. Fig. S24-Western blot analysis of KRAS in PBMC protein extracts. Fig. S25-STRING network analysis of the 67 significantly enriched proteins in

statin-pretreated, F-Az-treated samples. Fig. S26-STRING network analysis of the 22 significantly enriched proteins in non-statin-pretreated, GG-Az-treated samples.

Additional file 2: Tables S1, S6, S8-S10. Table S1-Summary of the identified proteins in the experiment with activated and non-activated Th1 cells, and in activated Th1 cells pretreated or not with statin. Table S6-Differentially expressed proteins in total extracts comparing activated and non-activated Th1 cells. Table S8-Differentially prenylated proteins comparing activated and non-activated Th1 cells. Table S9-Differentially expressed proteins in total extracts comparing activated Th1 cells pretreated or not with statin. Table S10-Differentially prenylated proteins comparing activated Th1 cells pretreated or not with statin.

Additional file 3: Tables S2-S5, S7. Table S2-Proteins with a discrepancy in the annotated and the experimental prenylation moiety. Table S3-Proteins with the new prenylation motifs CXXX, CXX, CX, and CCC. Table S4-Proteins with exactly one internal, potentially prenylated cysteine.
Table S5-The 49 proteins that were significantly less farnesylated upon FTI treatment. Table S7-The 63 proteins that were significantly differentially prenylated comparing activated and non-activated Th1 cells.

Acknowledgements
We are grateful to the donors who contributed to this study.

Authors' contributions
Conceptualization of study: JK, KB; design of experiments: JK, KF, KB; Conducting experiments: JK, CB, PW, SS, AH, KB; data analysis JK, AR, IW, DZ, KF, KB; writing and reviewing of manuscript: JK, AR, KB. All authors have read and approved the final manuscript.

Funding
This work has been supported by the Stiftung vormals Bündner Heilstätte Arosa, the Hans Groeber Foundation, the Swiss Institute of Allergy and Asthma Research (SIAF), and the Centers for Data Analysis, Visualisation, and Simulation (DAViS) and for Precision Proteomics Davos, funded by the Swiss Canton of Grisons.

Data availability
The mass spectrometry data generated and analysed during the present study are available in the MassIVE repository: Data from Experiment 1 (activated and non-activated Th1 cells) and Experiment 2 (activated Th1 cells pre-treated or not with statin) are available under the MassIVE ID MSV000095575 and can be accessed at: ftp://massive.ucsd.edu/v08/MSV000095575/ [81]. Data from the experiment with Th1 cells pre-treated or not with the farnesyl transferase inhibitor FTI-277 are available under the MassIVE ID MSV000096890, accessible at: ftp://massive-ftp.ucsd.edu/v09/MSV000096890/ [82]. The computational pipeline used for the analysis of prenylated proteins, along with all supplementary data, is available on GitHub: https://github.com/allru/prenylation_publication/tree/v1.0.0 and in the ETH Zurich Research Collection: https://www.research-collection.ethz.ch/handle/20.500.11850/728197 [83].

Declarations

Ethics approval and consent to participate
This study was conducted in accordance with the ethical principles outlined in the Declaration of Helsinki [80]. Ethics approval was obtained from the Ethics Commission of the Canton of Zurich under the protocol number BASEC ID: 2017–02065. Written informed consent to participate was obtained from all participants prior to their inclusion in the study.

Consent for publication
Not applicable.

Competing interests
The authors declare that they have no competing interests.

Author details
[1]Swiss Institute of Allergy and Asthma Research, University of Zurich, Davos, Switzerland. [2]Swiss Institute of Bioinformatics, Lausanne, Switzerland. [3]Institute for Theoretical Medicine, University of Augsburg, Augsburg, Germany. [4]ETH Library, ETH Zurich, Zurich, Switzerland. [5]Friedrich Miescher Institute for Biomedical Research, Basel, Switzerland.

Received: 25 March 2025 Accepted: 16 July 2025
Published online: 31 July 2025

References

1. Abbas AK, Lichtman AH, Pillai S. Cellular and molecular immunology. 10th ed. In: Antimicrobial agents and chemotherapy. Elsevier; 2022.
2. Su W, Chapman NM, Wei J, Zeng H, Dhungana Y, Shi H, et al. Protein prenylation drives discrete signaling programs for the differentiation and maintenance of effector Treg cells. Cell Metab. 2020;32(6):996-1011.e7. Available from: https://pubmed.ncbi.nlm.nih.gov/33207246/.
3. Stowers L, Yelon D, Berg LJ, Chant J. Regulation of the polarization of T cells toward antigen-presenting cells by Ras-related GTPase CDC42. Proc Natl Acad Sci U S A. 1995;92(11):562.
4. Du X, Zeng H, Liu S, Guy C, Dhungana Y, Neale G, et al. Mevalonate metabolism–dependent protein geranylgeranylation regulates thymocyte egress. J Exp Med. 2020;217(2): e20190969.
5. Thurnher M, Gruenbacher G. T lymphocyte regulation by mevalonate metabolism. Sci Signal. 2015;8(370). Available from: https://pubmed.ncbi.nlm.nih.gov/25829448/.
6. Swan G, Geng J, Park E, Ding Q, Zhou J, Walcott C, et al. A requirement of protein geranylgeranylation for chemokine receptor signaling and Th17 cell function in an animal model of multiple sclerosis. Front Immunol. 2021;12:12.
7. Stinchcombe JC, Barral DC, Mules EH, Booth S, Hume AN, Machesky LM, et al. Rab27a is required for regulated secretion in cytotoxic T lymphocytes. J Cell Biol. 2001;152(4):825.
8. Srikanth S, Kim KD, Gao Y, Woo JS, Ghosh S, Calmettes G, et al. A large Rab GTPase encoded by CRACR1A is a component of subsynaptic vesicles that transmit T cell activation signals. Sci Signal. 2016;9(420):ra31.
9. Miettinen TP, Björklund M. Mevalonate pathway regulates cell size homeostasis and proteostasis through autophagy. Cell Rep. 2015;13(11):2610-2620. https://doi.org/10.1016/j.celrep.2015.11.045.
10. Gomes AQ, Ali BR, Ramalho JS, Godfrey RF, Barral DC, Hume AN, et al. Membrane targeting of Rab GTPases is influenced by the prenylation motif. Mol Biol Cell. 2003;14(5):1882.
11. Lane KT, Beese LS. Thematic review series: lipid posttranslational modifications. Structural biology of protein farnesyltransferase and geranylgeranyltransferase type I. J Lipid Res. 2006;47(4):681.
12. Shirakawa R, Goto-Ito S, Goto K, Wakayama S, Kubo H, Sakata N, et al. A SNARE geranylgeranyltransferase essential for the organization of the Golgi apparatus. EMBO J. 2020;39(8):e104120. https://doi.org/10.15252/embj.2019104120.
13. Seabra MC, Goldstein JL, Südhof TC, Brown MS. Rab geranylgeranyl transferase: a multisubunit enzyme that prenylates GTP-binding proteins terminating in Cys-X-Cys or Cys-Cys. J Biol Chem. 1992;267(20):14497.
14. Thoma NH, Iakovenko A, Kalinin A, Waldmann H, Goody RS, Alexandrov K. Allosteric regulation of substrate binding and product release in geranylgeranyltransferase type II. Biochemistry. 2001;40(1):268.
15. Wang M, Casey PJ. Protein prenylation: unique fats make their mark on biology. Nat Rev Mol Cell Biol. 2016;17(2):110–22.
16. Resh MD. Trafficking and signaling by fatty-acylated and prenylated proteins. Nat Chem Biol. 2006;2:584.
17. Bateman A, Martin MJ, Orchard S, Magrane M, Ahmad S, Alpi E, et al. UniProt: the universal protein knowledgebase in 2023. Nucleic Acids Res. 2023;51:51(D1).
18. De Sandre-Giovannoli A, Bernard R, Cau P, Navarro C, Amiel J, Boccaccio I, et al. Lamin A truncation in Hutchinson-Gilford progeria. Science. 2003;300(5628):2055. https://doi.org/10.1126/science.1084125.
19. Eriksson M, Brown WT, Gordon LB, Glynn MW, Singer J, Scott L, et al. Recurrent de novo point mutations in lamin A cause Hutchinson-Gilford progeria syndrome. Nature. 2003;423(6937):293–8. Available from: https://www.nature.com/articles/nature01629.
20. Shackleton S, Smallwood DT, Clayton P, Wilson LC, Agarwal AK, Garg A, et al. Compound heterozygous ZMPSTE24 mutations reduce prelamin

A processing and result in a severe progeroid phenotype. J Med Genet. 2005;42(6):e36–e36. Available from: https://jmg.bmj.com/content/42/6/e36.
21. Berndt N, Hamilton AD, Sebti SM. Targeting protein prenylation for cancer therapy. Nat Rev Cancer. 2011;11(11):775. Available from: https://pmc.ncbi.nlm.nih.gov/articles/PMC4037130/.
22. Suzuki M, Jeng LJB, Chefo S, Wang Y, Price D, Li X, et al. FDA approval summary for lonafarnib (Zokinvy) for the treatment of Hutchinson-Gilford progeria syndrome and processing-deficient progeroid laminopathies. Genet Med. 2023;25(2):100335 Available from:https://www.sciencedirect.com/science/article/pii/S1098360022010036.
23. Jung D, Bachmann HS. Regulation of protein prenylation. Biomed Pharmacother. 2023;164:114915.
24. Ho AL, Brana I, Haddad R, Bauman J, Bible K, Oosting S, et al. Tipifarnib in head and neck squamous cell carcinoma with HRAS mutations. J Clin Oncol. 2021;39(17):1856–64.
25. Smith AE, Chan S, Wang Z, McCloskey A, Reilly Q, Wang JZ, et al. Tipifarnib potentiates the antitumor effects of PI3Kα inhibition in PIK3CA- and HRAS-dysregulated HNSCC via convergent inhibition of mTOR activity. Cancer Res. 2023;83(19):3252. Available from: https://pmc.ncbi.nlm.nih.gov/articles/PMC10543974/.
26. Karasic TB, Chiorean EG, Sebti SM, O'Dwyer PJ. A phase I study of GGTI-2418 (geranylgeranyl transferase I inhibitor) in patients with advanced solid tumors. Target Oncol. 2019;14(5):613. Available from: https://pmc.ncbi.nlm.nih.gov/articles/PMC7771543/.
27. Lerner EC, Qian Y, Blaskovich MA, Fossum RD, Vogt A, Sun J, et al. Ras CAAX peptidomimetic FTI-277 selectively blocks oncogenic Ras signaling by inducing cytoplasmic accumulation of inactive Ras-Raf complexes. J Biol Chem. 1995;270:270(45).
28. Kishore SP, Blank E, Heller DJ, Patel A, Peters A, Price M, et al. Modernizing the World Health Organization list of essential medicines for preventing and controlling cardiovascular diseases. J Am Coll Cardiol. 2018;71(5):564–74. Available from: https://www.jacc.org/10.1016/j.jacc.2017.11.056.
29. Blais JE, Wei Y, Yap KK, Alwafi H, Ma TT, Brauer R, et al. Trends in lipid-modifying agent use in 83 countries. Atherosclerosis. 2021;328:44–51. Available from: https://www.atherosclerosis-journal.com/action/showFullText?pii=S0021915021002525.
30. Guadamuz JS, Shooshtari A, Qato DM. Global, regional and national trends in statin utilisation in high-income and low/middle-income countries, 2015–2020. BMJ Open. 2022;12(9):e061350. Available from:https://bmjopen.bmj.com/content/12/9/e061350.
31. Vinci P, Panizon E, Tosoni LM, Cerrato C, Pellicori F, Mearelli F, et al. Statin-associated myopathy: emphasis on mechanisms and targeted therapy. Int J Mol Sci. 2021;22:11687.
32. Iwere RB, Hewitt J. Myopathy in older people receiving statin therapy: a systematic review and meta-analysis. Br J Clin Pharmacol. 2015;80(3):363. Available from: https://pmc.ncbi.nlm.nih.gov/articles/PMC4574822/.
33. Chakrabarti R, Engleman EG. Interrelationships between mevalonate metabolism and the mitogenic signaling pathway in T lymphocyte proliferation. J Biol Chem. 1991;266(19):12216.
34. Blank N, Schiller M, Krienke S, Busse F, Schätz B, Ho AD, et al. Atorvastatin inhibits T cell activation through 3-hydroxy-3-methylglutaryl coenzyme A reductase without decreasing cholesterol synthesis. J Immunol. 2007;179(6):3613.
35. Jameel A, Ooi KGJ, Jeffs NR, Galatowicz G, Lightman SL, Calder VL. Statin modulation of human T-cell proliferation, IL-1 β and IL-17 production, and IFN- γ T cell expression: synergy with conventional immunosuppressive agents. Int J Inflam. 2013;2013:434586.
36. Greenwood J, Steinman L, Zamvil SS. Statin therapy and autoimmune disease: from protein prenylation to immunomodulation. Nat Rev Immunol. 2006;6(5):358–70. Available from: Available from: https://pubmed.ncbi.nlm.nih.gov/16639429/.
37. Stefanou MI, Palaiodimou L, Katsanos AH, Milionis H, Kosmidou M, Lambadiari V, et al. The effects of HMG-CoA reductase inhibitors on disease activity in multiple sclerosis: a systematic review and meta-analysis. Mult Scler Relat Disord. 2022;58:58.
38. Palsuledesai CC, Ochocki JD, Markowski TW, Distefano MD. A combination of metabolic labeling and 2D-DIGE analysis in response to a farnesyltransferase inhibitor facilitates the discovery of new prenylated proteins. Mol Biosyst. 2014;10(5):1094.
39. Storck EM, Morales-Sanfrutos J, Serwa RA, Panyain N, Lanyon-Hogg T, Tolmachova T, et al. Dual chemical probes enable quantitative system-wide analysis of protein prenylation and prenylation dynamics. Nat Chem. 2019;11(6):552.
40. Palsuledesai CC, Ochocki JD, Kuhns MM, Wang YC, Warmka JK, Chernick DS, et al. Metabolic labeling with an alkyne-modified isoprenoid analog facilitates imaging and quantification of the prenylome in cells. ACS Chem Biol. 2016;11(10):2820.
41. Kho Y, Kim SC, Jiang C, Barma D, Kwon SW, Cheng J, et al. A tagging-via-substrate technology for detection and proteomics of farnesylated proteins. Proc Natl Acad Sci U S A. 2004;101(34):12479.
42. Suazo KF, Park KY, Distefano MD. A not-so-ancient grease history: click chemistry and protein lipid modifications. Chem Rev. 2021;121(12):7178–248. https://doi.org/10.1021/acs.chemrev.0c01108.
43. Berry AFH, Heal WP, Tarafder AK, Tolmachova T, Baron RA, Seabra MC, et al. Rapid multilabel detection of geranylgeranylated proteins by using bioorthogonal ligation chemistry. ChemBioChem. 2010;11(6):771–3. Available from: https://pubmed.ncbi.nlm.nih.gov/20209562/.
44. Charron G, Li MMH, MacDonald MR, Hang HC. Prenylome profiling reveals S-farnesylation is crucial for membrane targeting and antiviral activity of ZAP long-isoform. Proc Natl Acad Sci U S A. 2013;110(27):11085–90. https://doi.org/10.1073/pnas.1302564110?download=true.
45. Chan LN, Hart C, Guo L, Nyberg T, Davies BSJ, Fong LG, et al. A novel approach to tag and identify geranylgeranylated proteins. Electrophoresis. 2009;30(20):3598–606. Available from: https://pubmed.ncbi.nlm.nih.gov/19784953/.
46. Onono F, Subramanian T, Sunkara M, Subramanian KL, Peter Spielmann H, Morris AJ. Efficient use of exogenous isoprenols for protein isoprenylation by MDA-MB-231 cells is regulated independently of the mevalonate pathway. J Biol Chem. 2013;288(38):27444.
47. Armstrong SA, Hannah VC, Goldstein JL, Brown MS. CAAX geranylgeranyl transferase transfers farnesyl as efficiently as geranylgeranyl to RhoB. J Biol Chem. 1995;270(14):7864–8. Available from: https://pubmed.ncbi.nlm.nih.gov/7713879/.
48. Lebowitz PF, Davide JP, Prendergast GC. Evidence that farnesyltransferase inhibitors suppress Ras transformation by interfering with Rho activity. Mol Cell Biol. 1995;15(12):6613–22. Available from: https://pubmed.ncbi.nlm.nih.gov/8524226/.
49. Crooks GE, Hon G, Chandonia JM, Brenner SE. WebLogo: a sequence logo generator. Genome Res. 2004;14(6):1188–90. Available from: https://genome.cshlp.org/content/14/6/1188.full.
50. Sun JP, Luo Y, Yu X, Wang WQ, Zhou B, Liang F, et al. Phosphatase activity, trimerization, and the C-terminal polybasic region are all required for PRL1-mediated cell growth and migration. J Biol Chem. 2007;282(39):29043.
51. Varadi M, Anyango S, Deshpande M, Nair S, Natassia C, Yordanova G, et al. AlphaFold protein structure database: massively expanding the structural coverage of protein-sequence space with high-accuracy models. Nucleic Acids Res. 2022;50:50(D1).
52. Jumper J, Evans R, Pritzel A, Green T, Figurnov M, Ronneberger O, et al. Highly accurate protein structure prediction with AlphaFold. Nature. 2021;596(7873):583.
53. Bludau I, Willems S, Zeng WF, Strauss MT, Hansen FM, Tanzer MC, et al. The structural context of posttranslational modifications at a proteome-wide scale. PLoS Biol. 2022;20(5): e3001636.
54. van Kempen M, Kim SS, Tumescheit C, Mirdita M, Lee J, Gilchrist CLM, et al. Fast and accurate protein structure search with Foldseek. Nat Biotechnol. 2024;42(2):243.
55. Szklarczyk D, Kirsch R, Koutrouli M, Nastou K, Mehryary F, Hachilif R, et al. The STRING database in 2023: protein-protein association networks and functional enrichment analyses for any sequenced genome of interest. Nucleic Acids Res. 2023;51(D1):D638-46. Available from: https://pubmed.ncbi.nlm.nih.gov/36370105/.
56. Subramanian A, Tamayo P, Mootha VK, Mukherjee S, Ebert BL, Gillette MA, et al. Gene set enrichment analysis: a knowledge-based approach for interpreting genome-wide expression profiles. Proc Natl Acad Sci U S A. 2005;102(43):15545–50.
57. Mootha VK, Lindgren CM, Eriksson KF, Subramanian A, Sihag S, Lehar J, et al. PGC-1α-responsive genes involved in oxidative phosphorylation are coordinately downregulated in human diabetes. Nature Genetics.

2003;34(3):267–73. Available from: https://www.nature.com/articles/ng1180.
58. Troeger A, Chae HD, Senturk M, Wood J, Williams DA. A unique carboxyl-terminal insert domain in the hematopoietic-specific, GTPase-deficient Rho GTPase RhoH regulates post-translational processing. J Biol Chem. 2013;288(51):36451–62. Available from: https://pubmed.ncbi.nlm.nih.gov/24189071/.
59. Dorn T, Kuhn U, Bungartz G, Stiller S, Bauer M, Ellwart J, et al. RhoH is important for positive thymocyte selection and T-cell receptor signaling. Blood. 2007;109(6):2346–55. https://doi.org/10.1182/blood-2006-04-019034.
60. Katsuyama T, Li H, Krishfield SM, Kyttaris VC, Moulton VR. Splicing factor SRSF1 limits IFN-γ production via RhoH and ameliorates experimental nephritis. Rheumatology (Oxford). 2021;60(1):420–9. Available from: https://pubmed.ncbi.nlm.nih.gov/32810232/.
61. Tamehiro N, Nishida K, Sugita Y, Hayakawa K, Oda H, Nitta T, et al. Ras homolog gene family H (RhoH) deficiency induces psoriasis-like chronic dermatitis by promoting TH17 cell polarization. J Allergy Clin Immunol. 2019;143(5):1878–91 https://pubmed.ncbi.nlm.nih.gov/30339851/.
62. Li X, Bu X, Lu B, Avraham H, Flavell RA, Lim B. The hematopoiesis-specific GTP-binding protein RhoH is GTPase deficient and modulates activities of other Rho GTPases by an inhibitory function. Mol Cell Biol. 2002;22(4):1158–71. Available from: https://pubmed.ncbi.nlm.nih.gov/11809807/.
63. Fueller F, Kubatzky KF. The small GTPase RhoH is an atypical regulator of haematopoietic cells. Cell Commun Signal. 2008;6:6. Available from: https://pmc.ncbi.nlm.nih.gov/articles/PMC2565660/.
64. Baron R, Fourcade E, Lajoie-Mazenc I, Allal C, Couderc B, Barbaras R, et al. RhoB prenylation is driven by the three carboxyl-terminal amino acids of the protein: evidenced in vivo by an anti-farnesyl cysteine antibody. Proc Natl Acad Sci U S A. 2000;97(21):11626–31.
65. Kazi A, Vasiyani H, Ghosh D, Bandyopadhyay D, Shah RD, Vudatha V, et al. FGTI-2734 inhibits ERK reactivation to overcome sotorasib resistance in KRAS G12C lung cancer. J Thorac Oncol. 2025;20(3):331–44. Available from: http://www.ncbi.nlm.nih.gov/pubmed/39603412.
66. Forrester MT, Hess DT, Thompson JW, Hultman R, Moseley MA, Stamler JS, et al. Site-specific analysis of protein S-acylation by resin-assisted capture. J Lipid Res. 2011;52(2):393.
67. Suazo KF, Bělíček J, Schey GL, Auger SA, Petre AM, Li L, et al. Thinking outside the CaaX-box: an unusual reversible prenylation on ALDH9A1. RSC Chem Biol. 2023;4(11):913.
68. Lerner EC, Zhang TT, Knowles DB, Qian Y, Hamilton AD, Sebti SM. Inhibition of the prenylation of K-Ras, but not H- or N-Ras, is highly resistant to CAAX peptidomimetics and requires both a farnesyltransferase and a geranylgeranyltransferase I inhibitor in human tumor cell lines. Oncogene. 1997;15(11):1283–8. Available from: https://www.nature.com/articles/1201296.
69. Hirota Y, Nakagawa K, Sawada N, Okuda N, Suhara Y, Uchino Y, et al. Functional characterization of the vitamin K2 biosynthetic enzyme UBIAD1. PLoS One. 2015;10(4):e0125737. Available from: https://journals.plos.org/plosone/article?id=10.1371/journal.pone.0125737.
70. Schumacher MM, Elsabrouty R, Seemann J, Jo Y, DeBose-Boyd RA. The prenyltransferase UBIAD1 is the target of geranylgeraniol in degradation of HMG CoA reductase. Elife. 2015;2015(4):e05560.
71. Kulkarni AJ, Rodriguez-Coira J, Stocker N, Radzikowska U, García-Cívico AJ, Dolset MID, et al. L-phenylalanine is a metabolic checkpoint of human Th2 cells. bioRxiv. 2024;2024.07.29.605231. Available from: https://www.biorxiv.org/content/10.1101/2024.07.29.605231v1.
72. Baerenfaller K, Massonnet C, Walsh S, Baginsky S, Bühlmann P, Hennig L, et al. Systems-based analysis of Arabidopsis leaf growth reveals adaptation to water deficit. Mol Syst Biol. 2012;8: 606.
73. Cox J, Mann M. MaxQuant enables high peptide identification rates, individualized p.p.b.-range mass accuracies and proteome-wide protein quantification. Nat Biotechnol. 2008;26(12):1367–72. Available from: http://www.nature.com/finder/10.1038/nbt.1511.
74. Svozil J, Baerenfaller K. A cautionary tale on the inclusion of variable posttranslational modifications in database-dependent searches of mass spectrometry data. Methods Enzymol. 2017;586:433.
75. Zhang X, Smits AH, Van Tilburg GBA, Ovaa H, Huber W, Vermeulen M. Proteome-wide identification of ubiquitin interactions using UbIA-MS. Nat Protoc. 2018;13(3).
76. Gatto L, Lilley KS. Msnbase-an R/Bioconductor package for isobaric tagged mass spectrometry data visualization, processing and quantitation. Bioinformatics. 2012;28(2):288.
77. Ahlmann-Eltze C, Anders S. proDA: probabilistic dropout analysis for identifying differentially abundant proteins in label-free mass spectrometry. bioRxiv. 2020:661496. Available from: https://www.biorxiv.org/content/10.1101/661496v2.
78. Krystkowiak I, Manguy J, Davey NE. PSSMSearch: a server for modeling, visualization, proteome-wide discovery and annotation of protein motif specificity determinants. Nucleic Acids Res. 2018;46(W1):W235-41. https://doi.org/10.1093/nar/gky426.
79. Schrödinger LLC. The PyMOL molecular graphics system, version~1.8. 2015.
80. World Medical Association. World Medical Association declaration of Helsinki: ethical principles for medical research involving human subjects. JAMA. 2013;310(20):2191–4. Available from: https://pubmed.ncbi.nlm.nih.gov/24141714/.
81. Koch J, Baerenfaller K. Prenylation in Th1 cells assessed by click chemistry. Available from: ftp://massive-ftp.ucsd.edu/v08/MSV000095575/10.25345/C5X63BH4W.
82. Koch J, Baerenfaller K. Farnesylation in Th1 cells assessed by click chemistry. Available from: ftp://massive-ftp.ucsd.edu/v09/MSV000096890/10.25345/C50C4SX3W.
83. Koch J, Ruggia A, Beha C, Wipf I, Zhakparov D, Westermann P, et al. Supplementary code and data: "uncovering protein prenylation in Th1 cells: novel prenylation sites and insights into statin and farnesyltransferase inhibition". Available from: https://www.research-collection.ethz.ch/handle/20.500.11850/72819710.3929/ethz-b-000728197.

Publisher's Note